2018 Doctor Thesis

Structure refinement of Al-coated Mg-Li alloy by multi extrusion-rolling process and its superplastic characteristics

Tianlong Zhang

Hokkaido University

Graduate School of Engineering

Division of Material Science and Engineering

TABLE OF CONTENTS

Chapter 1 Introduction

1.1 Mg and Mg alloys

Magnesium is one of the lightest metals with a low density of 1.7 g/cm^3. It has a hexagonal crystal structure with a = 0.320 nm, c = 0.520 nm, c/ a = 1.624. The basal plane is close-packed, and the axial ratio is only slightly greater than the theoretical value for incompressible spheres [1.1].

Mg alloys are potential structural metal materials which can meet the compelling need for light-weighting and energy-efficiency in industry. It is reported that a weight reduction of 22.5 kg will improve fuel efficiency by around 1% in a typical car [1.2]. Fig. 1.1 gives the densities of usually used metal materials. Mg is approximately 30% lighter than Al and 80% lighter than Fe. Also, Mg has high thermal conductivity, high dimensional stability, good electromagnetic shielding characteristics, high damping characteristics, good machinability and can be easily recycled [1.3]. Moreover, Mg is the eighth most abundant element on earth. Especially, Mg is very rich in the sea water. Each cubic meter of the sea water contains approximately 1.3 kg Mg [1.4]. Mg alloys are usually applied in aerospace, automotive and electronic industries where weight reduction is important. Auto manufacturing companies have made the most of research and development on Mg and its alloys [1.5, 1.6]. Fig 1.2 displays some examples of the automotive components made of Mg alloys instead of alternative materials, by which 22% to 70% weight reduction is possible [1.4]. Weight reduction not only saves

energy, but it also reduces greenhouse gas emissions. Therefore, it is of both economic and environmental benefits to develop Mg alloys.

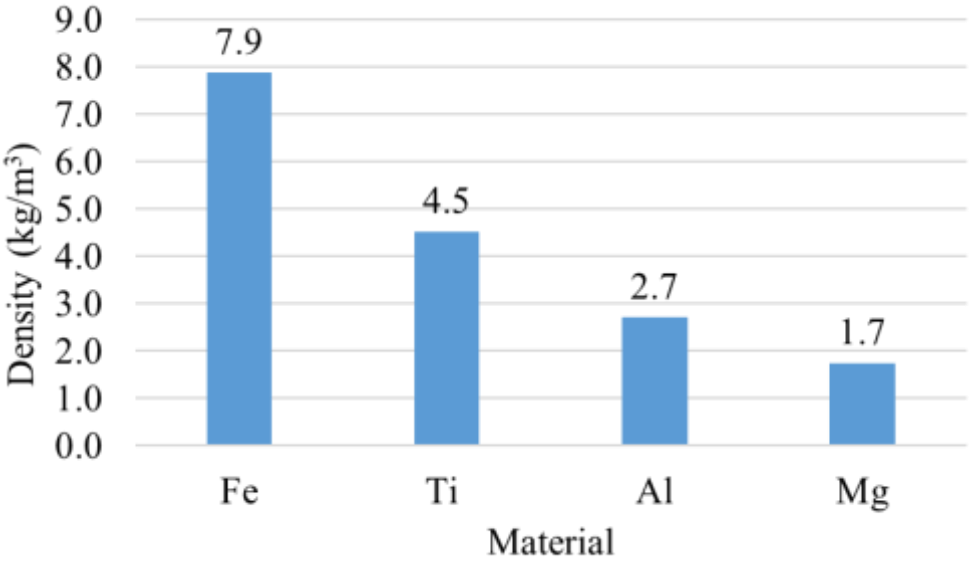

Fig. 1.1 Densities of the structural metal materials

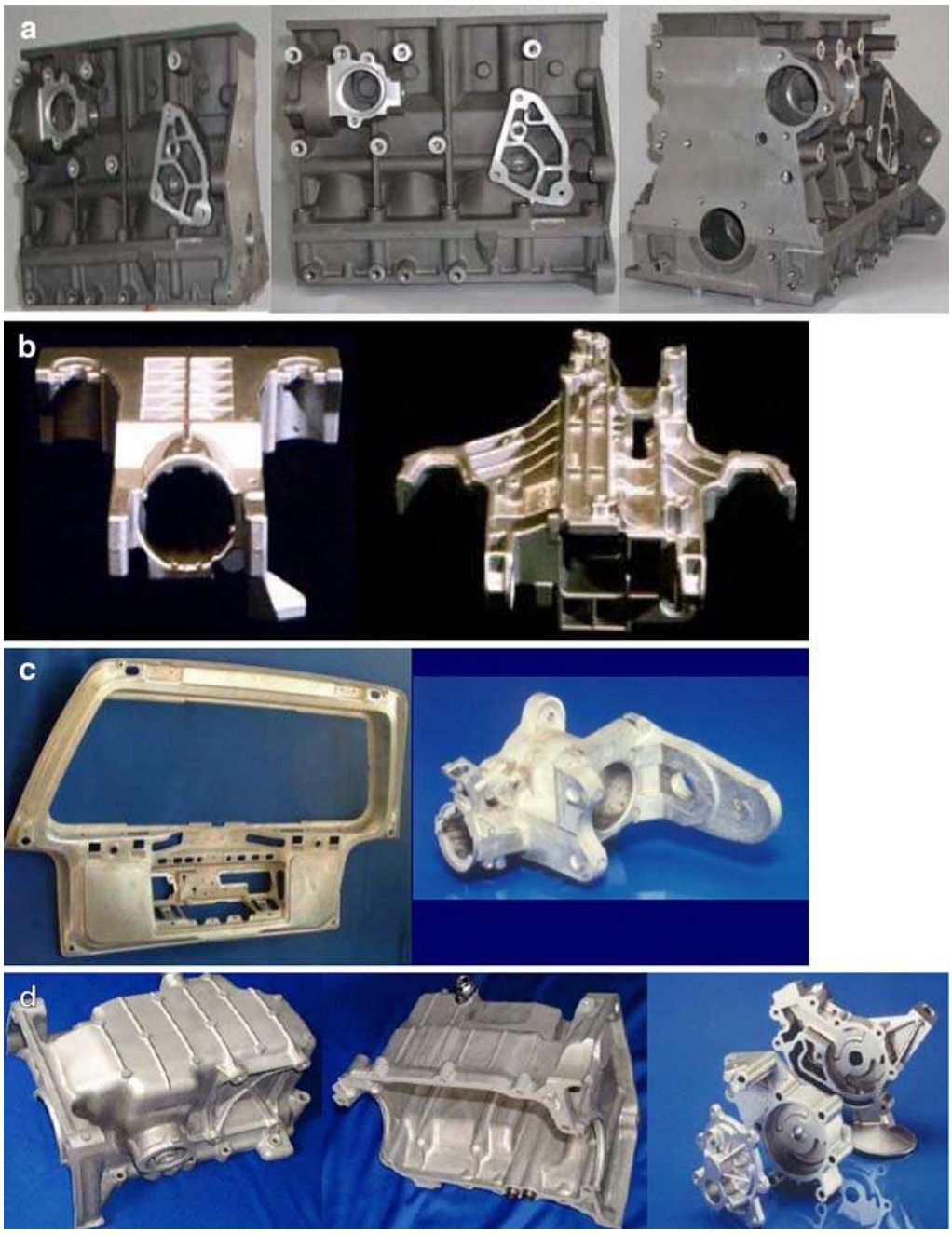

Fig. 1.2 Examples of automotive components made of Mg alloys (a: Engine block, b: Steering column module, c: Door frame and key lock housing, d: Oil pan).

1.2 Problems of Mg alloys

In spite of those attractive advantages described above, Mg alloys have some undesirable properties. Poor corrosion resistance and low formability are the most critical challenges in the use of Mg alloys, as described below.

1.2.1 Corrosion resistance of Mg alloys

Low corrosion resistance is a critical problem in the use of Mg alloys, particularly for outdoor applications. Due to an extremely high chemical activity, Mg and its alloys are significantly susceptible to galvanic corrosion, which can cause severe pitting in the metal and result in decreased mechanical stability and an unattractive appearance [1.7].

The overall corrosion reaction of Mg in aqueous environments can be expressed by [1.8]:

$$Mg + 2H_2O \rightarrow Mg(OH)_2 + H_2 \quad (1\text{-}1)$$

This overall reaction can be divided into the following partial reactions:

$$Mg \rightarrow Mg^{2+} + 2e^- \text{ (anodic reaction)} \quad (1\text{-}2)$$

$$2H_2O + 2e^- \rightarrow H_2 + 2OH^- \text{ (cathodic reaction)} \quad (1\text{-}3)$$

$$Mg^{2+} + 2OH^- \rightarrow Mg(OH)_2 \text{ (product formation)} \quad (1\text{-}4)$$

Mg alloys also have similar corrosion reactions to those of pure Mg, fundamentally. For example, for Mg-Al-Zn alloys, Mg is still the main component dissolving into solution [1.9].

Another reason of the low corrosion of Mg alloys is their low-quality oxide films. Mg has the lowest standard potential of all the engineering metals as illustrated in Fig. 1.3 [1.10]. Therefore, Mg alloys are easily oxidized, and their surfaces are always covered with oxide films when they are exposed in Air. These oxide films can sometimes provide good corrosion resistance. For example, Al has good corrosion resistance in ambient environment because of its dense and stable oxide film, though Al itself is very active metal. However, magnesium oxide, MgO, inherently lacks the chemical stability in a humid atmosphere, and reacts slowly with water to form $Mg(OH)_2$ films [1.11]. Therefore, the surface films of Mg alloys are not dense and strong enough to provide a good corrosion resistance as those of Al alloys.

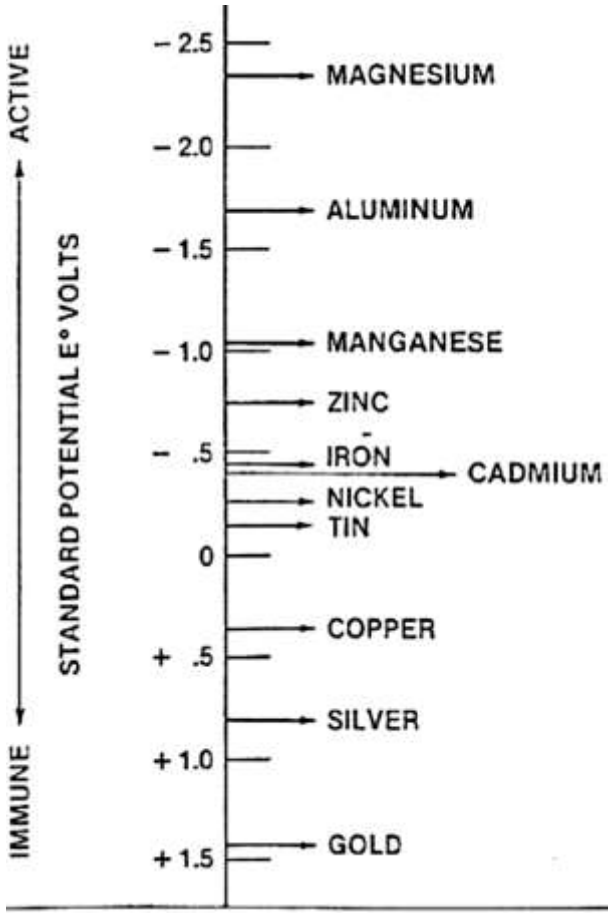

Fig. 1.3 Standard potential of engineering metals [1.10]

One of the most effective ways to prevent corrosion of Mg alloys is to coat the base materials with other corrosion-resistant materials. Coatings can protect the Mg alloy substrates by providing barriers between the substrates and the outside environment. For a coating to provide adequate protection, the coating must be uniform, well adhered, pore free and damage-resistant. There have been many technologies available for coating Mg alloys, such as electrochemical plating, conversion coatings, anodizing, hydride coatings, organic coatings and vapor-phase processes. However, because of the extremely active chemical property of Mg, many traditional coating methods

do not work well on Mg alloys. Two of the most common examples, plating and anodizing are introduced in detail as below:

One of the most effective and simple techniques for introducing a metallic coating is electrochemical plating. Electrochemical plating can alter the surface of a metal to another one which usually exhibits good corrosion. Though plating of Mg alloy has been shown to be useful in a number of applications [1.12-1.14], Mg is considered to be one of the most metal difficult to be plated due to its high reactivity. Moreover, in air, Mg quickly forms a passive oxide layer. This layer should be removed before plating to get a good adhesion and a uniform coverage of coating. Therefore, pretreatment processes are always required, which are always difficult and complex procedures. This results that the existing plating techniques are not efficient and not widely applicable.

Anodizing is an electrolytic process for producing an artificial corrosion-resistant oxide film on metals [1.15]. These oxide films usually exhibit good corrosion resistance, wear resistance and hardness. However, because of the phase separation in Mg alloys, the anodic coatings on Mg alloy tend to be inhomogeneous. When the coating is inhomogeneous, or it has defects, the corrosion of the base Mg alloy cannot be enhanced [1.16]. Additionally, the coating produced by anodizing is often brittle, which limits the application of the coated parts, especially in deformation process.

Traditional coating methods are not effective and efficient for Mg alloys, mainly because of the chemical property of Mg. Therefore, avoiding the use of

chemical methods should be reasonable. Mechanical methods can be used instead.

Mechanical coating methods have been reported. The most widely reported method is to produce a sandwich structure of corrosion-resistant metal/Mg alloy/corrosion-resistant metal by rolling [1.17]. This is a simple method to produce, for example, an Al-coated Mg alloy sheet with a quite good corrosion resistance. By this way, many problems existing in the chemical methods, such as inhomogeneity and brittleness of the coating, are successfully avoided. However, adhesion between the coating and the base alloy is not strong enough. During the further tensile deformation of this sandwich-structure composite, debonding of the coating occurs [1.17].

A new mechanical method was developed by the author's group by using the hot extrusion [1.18]. By this method, the coating and the Mg alloy exhibited a much better bonding even after a large tensile deformation [1.19]. In this method, pure Al was used as the coating material for its lightness and good corrosion resistance. In the hot extrusion process, Al and Mg alloys were plastically deformed in contact with each other at elevated temperatures and under a high pressure. After the extrusion, they were strongly bonded with each other. The details of this method will be introduced in chapter 2.

1.2.2 Formability of Mg alloys

Mg alloys generally have low ductility at room temperature because of the limited slip systems in the hexagonal close-packed (HCP) lattice structure

of Mg [1.20, 1.21]. This makes Mg alloys difficult to be deformed, which restricts their application. A solution of this problem is to add Li into Mg, which can change the structure of Mg from HCP to body-centered cubic (BCC). According to Mg-Li binary phase diagrams, as the concentration of Li increases, the stable phase changes from HCP (<5.5 wt.% Li) to HCP/BCC (5.5 wt.% − 10.3 wt.% Li) and further to BCC (>10.3 wt.% Li) [1.22]. Mg-Li alloys have lower densities (1.35 − 1.65 g/cm^3) than conventional Mg alloys [1.23]. Furthermore, the ductility of Mg-Li alloys has a large improvement when the content of Li is higher than 5.5 wt.%, because of the transition of HCP phases to BCC phases. The improvement of ductility gives Mg-Li alloys better formability than conventional Mg alloys at room temperature.

At high temperatures, Mg alloys can be more easily deformed. Furthermore, many Mg alloys are reported to exhibit the superplasticity at elevated temperatures [1.24-1.26]. The superplasticity is a special mechanical property in polycrystalline materials which can exhibit an extremely large elongation without any obvious necking [1.27]. Therefore, a potential effective solution of the formability problem of Mg alloy is the superplastic forming (SPF), which can be used to form many complex shapes in industry.

Grain boundary sliding (GBS) is generally accepted to be the mechanism that controls the superplastic deformation process [1.28]. To promote GBS is important to achieve a good superplasticity. Generally, finer structures bring about more GBS and better superplasticity. Structure refinement and control of grain size is the key point. To realize it, on one hand, dual-phase structure alloys can be used. In the alloy with the dual-phase structure, the existence of

phase boundary can effectively promote the GBS by limiting the grain growth. As stated above, the Mg-Li alloy becomes a dual-phase alloy when the composition of Li is 5.5 wt.% − 10.3 wt.%. A Mg-8 wt.% Li alloy has approximately equal volume fractions of the two phases, which is the best for superplasticity [1.29]. On the anther hand, grain size can be refined by plastic deformation. However, conventional plastic deformation methods like rolling and extrusion only have limited amount of deformation. Recently, severe plastic deformation methods e.g. accumulative roll bonding (ARB), equal channel angular extrusion (ECAE) have been developed to produce much larger deformation and ultra-fine grains [1.30]. However, these existing methods cannot effectively refine the coarse phases in the dual-phase Mg-Li alloys [1.31-1.35]. Therefore, a new plastic deformation method named multi extrusion-rolling process is developed to solve the problem in this thesis. The detail of this method will be introduced in chapter 6.

1.3 Motivation

The main subject of this thesis is to solve the two critical problems of Mg alloys: low corrosion resistance and low formability. Briefly, the hot extrusion coating method is to be used to better the corrosion resistance and the newly developed multi extrusion-rolling deformation process is to be used to refine the structure and improve the formability.

In fact, the solutions of these two problems are closely involved with each other. When the hot extrusion method is used to produce coating, the

product is a bar. When more kinds of shapes are desired, the bar should be further formed. Therefore, a good formability of the bar is very important. And how to form it into various kinds of shapes is important to its practical application. Comparing the hot extrusion method with the traditional chemical methods, we can find the main problem of the extrusion method: chemical coating method generally give coating on the completed parts with the finally desired shapes; however, by the hot extrusion method, in most cases, the coated bar still needs to be formed after the coating step.

Therefore, in this study, the feasibility of the fabrication of sheets from the bars is checked, for sheets are more widely used to form kinds of shapes and are also essential for SPF. After this, it will be investigated to develop the Al-coated Mg-Li alloy sheets with an excellent plasticity and even superplasticity for the possibility to form complex shapes. For this purpose, the newly developed multi extrusion-rolling process will be proposed to refine the structure of the Mg-Li alloy and to achieve a good formability.

1.4 Organization of this thesis

This thesis consists of 7 chapters and the organization is described below.

From chapter 2 to chapter 4, the fabrication and characterization of the Al-coated Mg-8Li alloy are introduced. In fact, three kinds of dual-phase Mg-Li alloys are used in this study: Mg-8Li (LZ80), Mg-8Li-2Zn (LZ82) and Mg-8Li-5Zn (LZ85). They exhibit similar behaviors and characteristics in the

fabrication process, so only LZ80 alloy is taken as the example and discussed in detail in chapters 2, 3 and 4.

In chapter 2, the coating method by hot extrusion is introduced and the characterization of the as-extruded Al-coated LZ80 alloy is illustrated.

In chapter 3, the as-extruded Al-coated LZ80 alloy bars are deformed into sheets by hot rolling. The feasibility is checked, and the microstructure and corrosion resistance are investigated.

In chapter 4, the tensile properties of the Al-coated LZ80 alloy sheet are investigated, both at room temperature and elevated temperatures. The superplastic tensile properties are investigated with special attention.

Chapter 5 briefly lists the comparison of the tensile properties between the Al-coated LZ80, LZ82 and LZ85 alloy sheets to find the best choice for practical application with high comprehensive mechanical properties.

In chapter 6, the microstructure of the Mg-Li alloy is refined by the multi extrusion-rolling process to develop a better superplasticity. Careful discussion is made on the superplastic mechanism.

Finally, in chapter 7, the contributions and future perspectives of this study are summarized.

References

[1.1] E. F. Emley, Principles of Magnesium Technology, Perga-mon Press New York 1966.

[1.2] T. M. Pollock, Weight loss with magnesium alloys, Science 328 (2010) 986-987.

[1.3] Y. Kojima, Project of Platform Science and Technology for Advanced Magnesium Alloys, Mater. Trans. 42 (2001) 1154-1159.

[1.4] M. K. Kulekci, Magnesium and its alloys applications in automotive industry, Int. J. Adv. Manuf. Technol. 39 (2008) 851-865.

[1.5] C. Blawert, N. Hort, K. V. Kainer, Automotive applications of magnesium and its alloy, Trans. Indian. Inst. Met. 57 (2004) 397-408.

[1.6] H. Friedrich, S. Schumann, Research for a “new age of magnesium” in the automotive industry, J. Mater. Process. Technol. 117 (2001) 276-281.

[1.7] J. E. Gray, B. Luan, Protective coatings on magnesium and its alloys — a critical review, J. Alloys Compd. 336 (2002) 88-113.

[1.8] G. L. Makar, J. Kruger, Corrosion of magnesium, Int. Mater. Rev. 38 (1993) 138-153

[1.9] G. Song, A. Atrens, X. Wu, Z. Bo, B. Zhang, Corrosion behaviour of AZ21, AZ501 and AZ91 in sodium chloride, Corr. Sci. 40 (1998), 1769-1791.

[1.10] G. L. Song, A. Atrens, Corrosion mechanisms of magnesium alloys, Adv. Eng. Mater. 1 (1999) 11-33.

[1.11] O. Frühwirth, G. W. Herzog, I. Hollerer, A. Rachetti, Dissolution and hydration kinetics of MgO, Surf. Technol. 24 (1985) 301-317.

[1.12] J. L. Luo, N. Cui, Effects of microencapsulation on the electrode behavior of Mg_2Ni-based hydrogen storage alloy in alkaline solution, J. Alloys Comp. 264 (1998) 299-305.

[1.13] J. Chen, D. H. Bradhurst, S. X. Dou, H. K. Liu, The effect of chemical coating with Ni on the electrode properties of Mg_2Ni alloy, J. Alloys Comp. 280 (1998) 290-293.

[1.14] C. Y. Wang, P. Yao, D. H. Bradhurst, H. K. Liu, S. X. Dou, Surface modification of Mg_2Ni alloy in an acid solution of copper sulfate and sulfuric acid, J. Alloys Comp. 285 (1999) 267-271.

[1.15] Y. J. Zhang, C. W. Yan, F. H. Wang, H. Y. Lou, C. A. Cao, Study on the environmentally friendly anodizing of AZ91D magnesium alloy, Surf. Coat. Technol. 161 (2002) 36-43.

[1.16] A. K. Sharma, R. Uma Rani, K. Giri, Studies on anodization of magnesium alloy for thermal control applications, Metal Finishing 95 (1997) 43.

[1.17] H. Matsumoto, S. Watanabe, S. Hanada, Fabrication of pure Al/Mg-Li alloy clad plate and its mechanical properties, J. Mater. Process. Technol. 169 (2005) 9-15.

[1.18] T. Tokunaga, K. Matsuura, M. Ohno, Aluminum coating on magnesium-based alloy by hot extrusion and its characteristics, Materials Transactions, 53 (2012) 1134-1041.

[1.19] T. Tokunaga, K. Matsuura, M. Ohno, Superplastic behavior of Al-coated Mg alloy sheet, J. Alloys Compd. 601 (2014) 179-185.

[1.20] M. R. Barnett, Twinning and the ductility of magnesium alloys Part II. "Contraction" twins, Mater. Sci. Eng. A 464 (2007) 1-7.

[1.21] J. Koike, Enhanced deformation mechanisms by anisotropic plasticity in polycrystalline mg alloys at room temperature, Metall. Mater. Trans. A 36 (2005) 1689-1696.

[1.22] A. A. Nayeb-Hashemi, J. B. Clark, A. D. Pelton, The Li-Mg (Lithium-Magnesium) System, Bull. Alloy Ph. Diagr. 5 (1984) 365-374.

[1.23] R. Wu, Y. Yan, G. Wang, L. E. Murr, W. Han, Z. Zhang, M. Zhang, Recent progress in magnesium-lithium alloys, Int. Mater. Rev. 2 (2015) 65-100

[1.24] L. Zhang, J. H. Zhang, C. Xu, S. J. Liu, et al. Investigation of high-strength and superplastic Mg-Y-Gd-Zn alloy, Mater. Des. 61 (2014) 168-176.

[1.25] R. Alizadeh, R. Mahmudi, A. H. W. Ngan, Y. Huang, T. G. Langdon, Superplasticity of a nano-grained Mg-Gd-Y-Zr alloy processed by high-pressure torsion, Mater. Sci. Eng. A 651 (2016) 786-794.

[1.26] X. H. Liu, R. Z. Wu, Z. Y. Niu, J. H. Zhang, M. L. Zhang, Superplasticity at elevated temperature of an Mg-8%Li-2%Zn alloy, J. Alloys Compd. 541 (2012) 372-375.

[1.27] M. Kawasaki, R. B. Figueiredo, T. G. Langdon, The requirements for superplasticity with an emphasis on magnesium alloys, Adv. Eng. Mater. 18 (2016) 127-131.

[1.28] T. G. Langdon, An evaluation of the strain contributed by grain boundary sliding in superplasticity, Mater. Sci. Eng. A 174 (1994) 225-230.

[1.29] F. R. Cao, J. Z. Cui, J. L. Wen, F. Lei, Mechanical behaviour and microstructure evolution of superplastic Mg-8.4 wt pct Li alloy and effect of grain size and phase ratio on its elongation, J. Mater. Sci. Technol. 16 (2000) 55-58.

[1.30] A. Azushima, R. Kopp, A. Korhonen, D. Y. Yang, F. Micari, G. D. Lahoti, P. Groche, J. Yanagimoto, N. Tsuji, A. Rosochowski, A. Yanagida, Severe plastic deformation (SPD) processes for metals, CIRP Ann-Manuf. Techn. 57 (2008) 716-735.

[1.31] X. H. Liu, H. B. Zhan, S. H. Gu, Z. K. Qu, R. Z. Wu, M. L. Zhang, Superplasticity in a two-phase Mg-8Li-2Zn alloy processed by two-pass extrusion, Mater. Sci. Eng. A 528 (2011) 6157-6162.

[1.32] T. Z. Wang, H. P. Zheng, R. Z. Wu, J. L. Yang, X. D. Ma, M. L. Zhang, Preparation of fine-grained and high-strength Mg-8Li-3Al-1Zn alloy by accumulative roll bonding, Adv. Eng. Mater. 18 (2016) 304-311.

[1.33] L. G. Hou, T. Z. Wang, R. Z. Wu, J. H. Zhang, M. L. Zhang, A. P. Dong, B. D. Sun, S. Betsofen, B. Krit, Microstructure and mechanical properties of Mg-5Li-1Al sheets prepared by accumulative roll bonding, J. Mater. Sci. Technol. 34 (2018) 317-323.

[1.34] H. P. Yang, M. W. Fu, S. To, G. C. Wang, Investigation on the maximum strain rate sensitivity (m) superplastic deformation of Mg-Li based alloy, Mater. Des. 112 (2016) 151-159.

[1.35] X. S. Fu, Y. Yang, J. W. Hu, J. F. Su, X. P. Zhang. X. D. Peng, Microstructure and mechanical properties of as-cast and extruded Mg-8Li-1Al-0.5Sn alloy, Mater. Sci. Eng. A 709 (2018) 247-253.

Chapter 2 Coating by hot extrusion

2.1 Introduction

As introduced in chapter 1, the hot extrusion method is used to give an Al coating on the Mg-Li alloy. In this chapter, the method will be illustrated in detail and the results will be displayed and discussed.

Fig. 2.1 illustrates why the mechanical method like extrusion can bond the Al coating with the Mg-Li alloy substrate. In normal state, the oxide films on the surfaces of the metals prevent the bonding of two metals. However, the metal is usually much more ductile than its oxide film. As shown in Fig. 2.1, when giving the metals a large deformation and pressure at the same time, the oxide films are broken, and the metals can be bonded to each other with the fresh surfaces without oxide films. Therefore, how much new surfaces can be produced is essentially important and the extrusion can bring about large fresh surfaces. This is reason why the hot extrusion method can give a good bonding between the coating and the substrate.

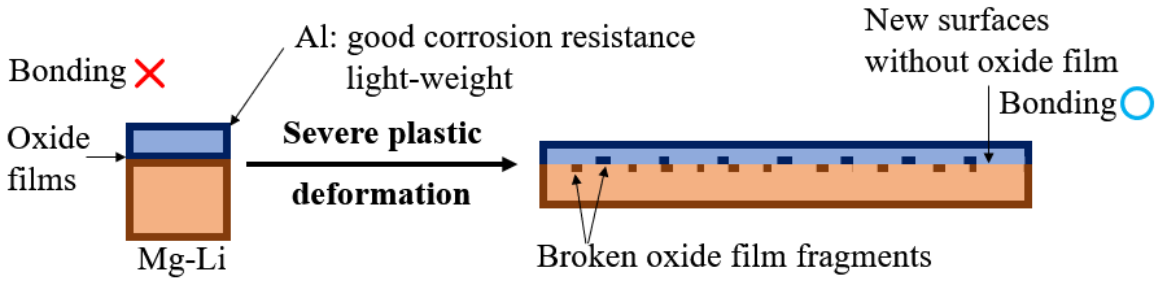

Fig. 2.1 Schematic illustration of the mechanical coating method.

2.2 Experimental

Fig. 2.2 schematically illustrates the hot extrusion equipment used in this study. A Mg-Li alloy billet was put in the bottom of the container, and a 5 mm-thick Al plate (99.99 wt.% purity) was placed between the die and the Mg-Li alloy billet. A Mg-8 wt% Li alloy was employed in this study. The size and shape of the die are shown in Fig. 2.3. Before extrusion, the die and rams were pre-heated to 548 K outside the container, while the container was pre-heated to 473 K. Then, the Mg-Li alloy billet and the Al plate were put into the container, and the die and rams were set on to the Al plate as illustrated in Fig. 2.2. After this setting, the temperature of the container was increased from 473 to 523 K and the extrusion was carried out by pressing the rams downward. The pressure was 190 MPa and the ram speed was 0.6 mm/s. This extrusion was an indirect extrusion and the billet was extruded upward together with the Al. After extrusion, the as-extruded bar was cut every 10 mm in the longitudinal direction from the tip to the end in order to measure the thickness of the Al coating on the cross section. Five thickness values measured on each long side of rectangular cross section were used to calculate the average.

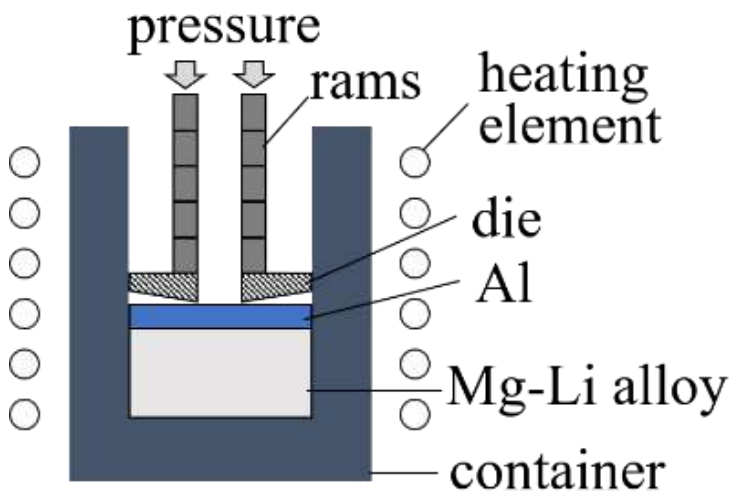

Fig. 2.2 Schematic illustration of the hot extrusion equipment.

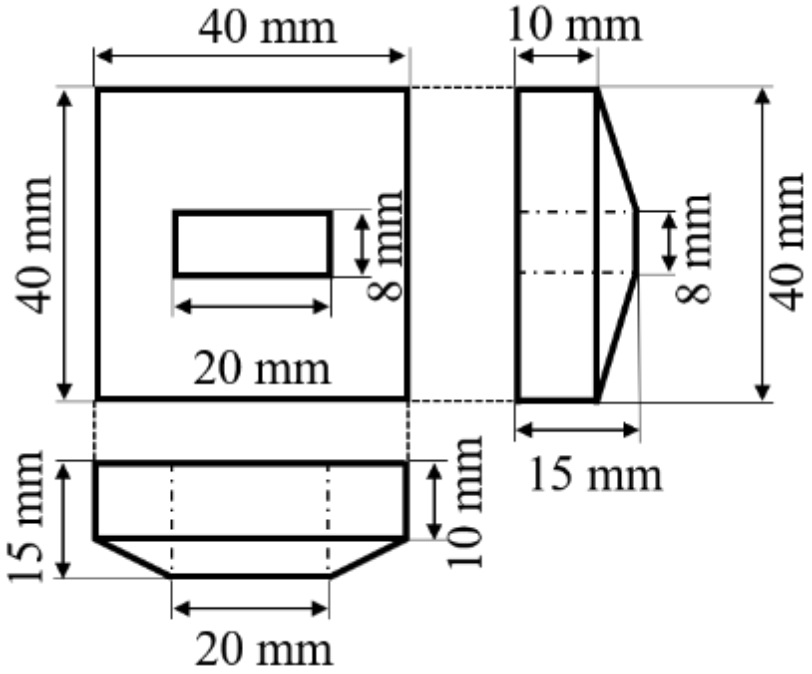

Fig. 2.3 Schematic drawing of the die.

The microstructures of the samples were observed by using an optical microscope (OM). To distinguish α phase and β phase in the Mg-Li alloy substrate, some samples were etched with a mixture of picric acid of 32 mL, acetic acid of 20 mL, distilled water of 20 mL, and ethyl alcohol of 18 mL before observation.

The corrosion resistance was evaluated by an immersion test as shown in Fig 2.4. The sample was immersed in a 0.5 mass% HCl aqueous solution for 90 minutes at room temperature and their weight loss per unit area was monitored during the immersion. Before immersion, the surfaces of the sample except the Al coating surface were covered with resin, which does not react with the acid. For a comparison, Mg-Li alloy without Al coating and the pure Al were also subjected to this corrosion test.

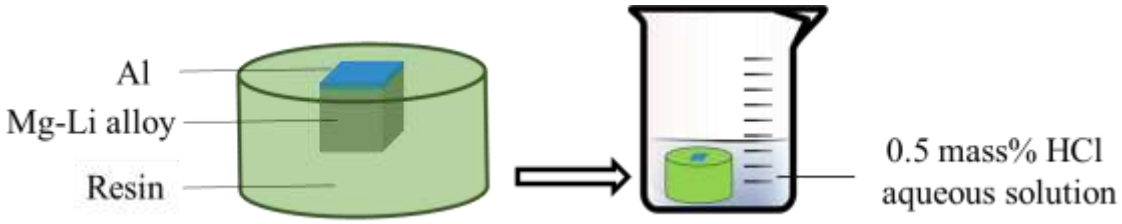

Fig. 2.4 Schematic illustration of the corrosion test

2.3 Results and discussions

2.3.1 Microstructure of the Al-coated Mg-Li alloy bar

Fig. 2.5 shows the appearance of the as-extruded Al-coated Mg-Li alloy bar. The bar has a smooth surface and no defect can be observed. Fig. 2.6 (a) shows the cross section of the bar. The Al coating is uniformly coated on the

Mg-Li alloy substrate. Fig. 2.6 (b) illustrates the interface between the Al coating and the Mg-Li alloy substrate. In the Mg-Li alloy substrate, the bright and the dark areas are α (HCP, Mg-rich) and β (BCC, Li-rich) phases, respectively. In Fig. 2.6 (b), no cracks are observed at the interface, which suggests a good bonding between the Al coating and the Mg-Li alloy substrate. Fig. 2.7 demonstrates the change of the Al coating thickness in the longitudinal direction from the tip of the as-extruded bar. The thickness of the coating near the tip is particularly thick, because at the start of the extrusion the thick Al plate covers the top of the Mg-Li alloy billet. As the extrusion proceeds, the thickness of the coating decreases and becomes uniform at around 200 μm from a position about 50 mm away from the tip.

Fig. 2.5 Appearance of the as-extruded Al-coated Mg-Li alloy bar

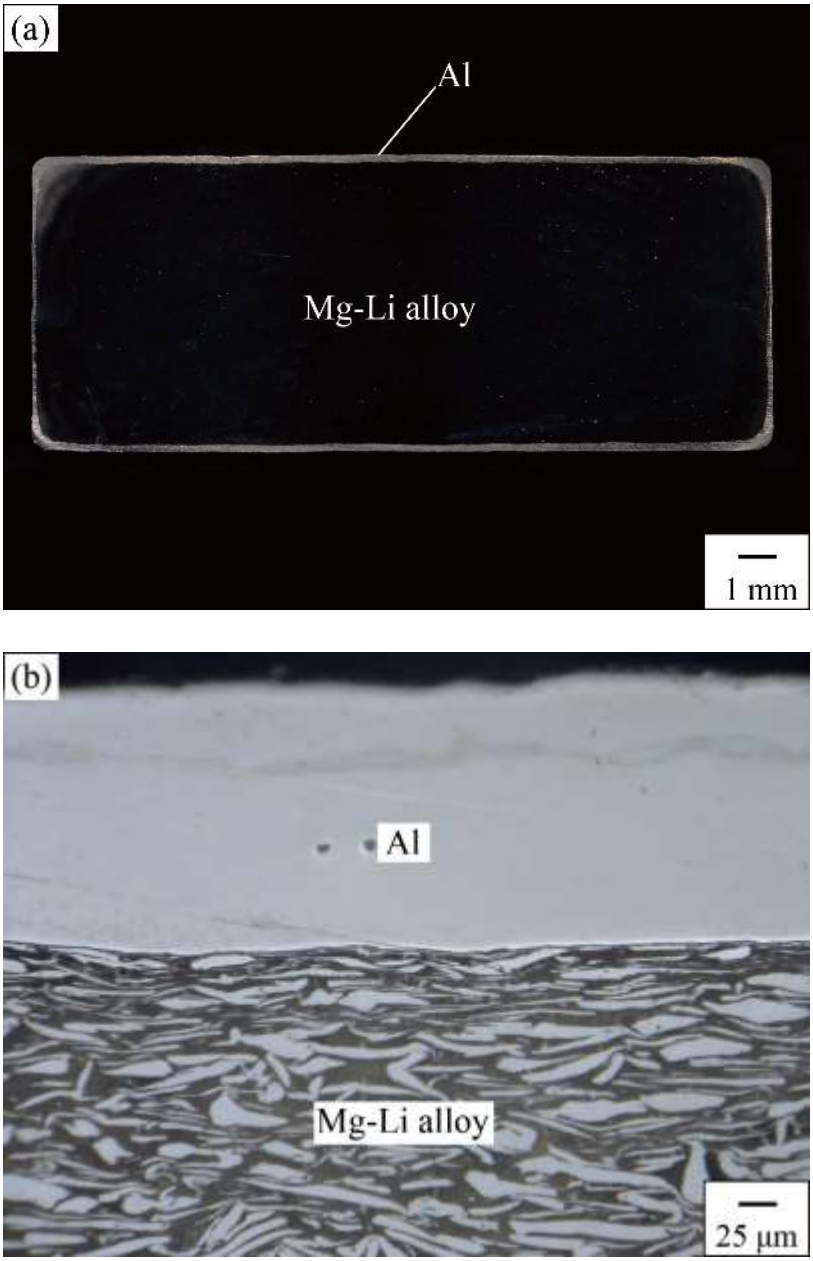

Fig. 2.6 (a) Cross section of the as-extruded Al-coated Mg-Li alloy rectangular bar which is about 50 mm from the tip, and (b) interface between Al coating and Mg-Li alloy substrate in the cross section. The extrusion direction corresponds to the normal to the figure.

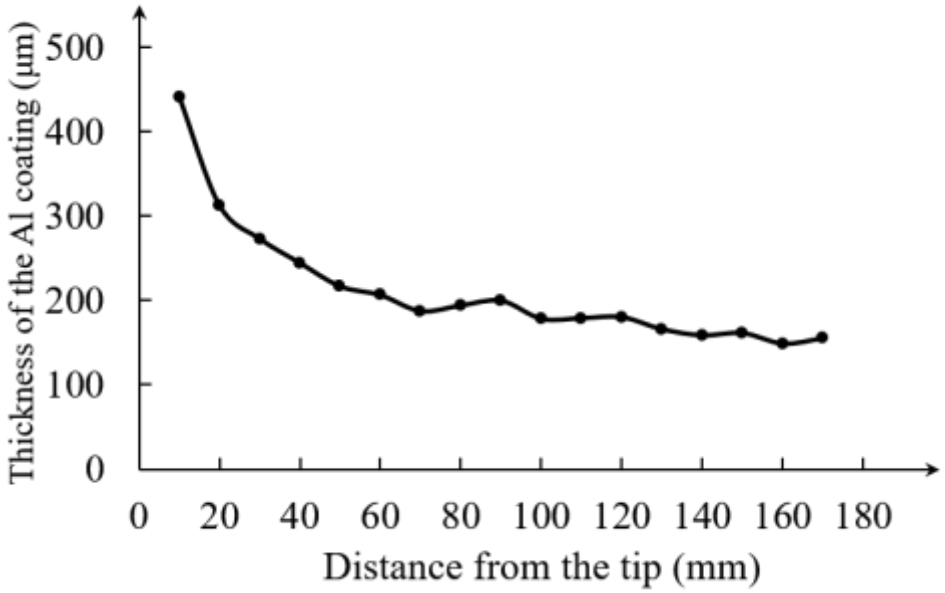

Fig. 2.7 Change of the coating thickness in the longitudinal direction of the as-extruded Al-coated Mg-Li alloy bar.

2.3.2 Corrosion resistance of Al-coated Mg-Li alloy bar

Fig. 2.8 displays the results of the corrosion tests, which gives the weight losses of different samples during immersion in a 0.5 mass% HCl aqueous solution at room temperature. Without the Al coating, as marked by the circle, the Mg-Li alloy reacts with the acid solution seriously and loses its weight gradually with the increase of the immersion time. However, the sample of the as-extruded Al-coated Mg-Li alloy bar shows no weight loss in the HCl solution, which is the same as the result of pure Al. Therefore, it suggests that an excellent corrosion resistance can be given to the Mg-Li alloy by the Al coating by using the present hot extrusion method.

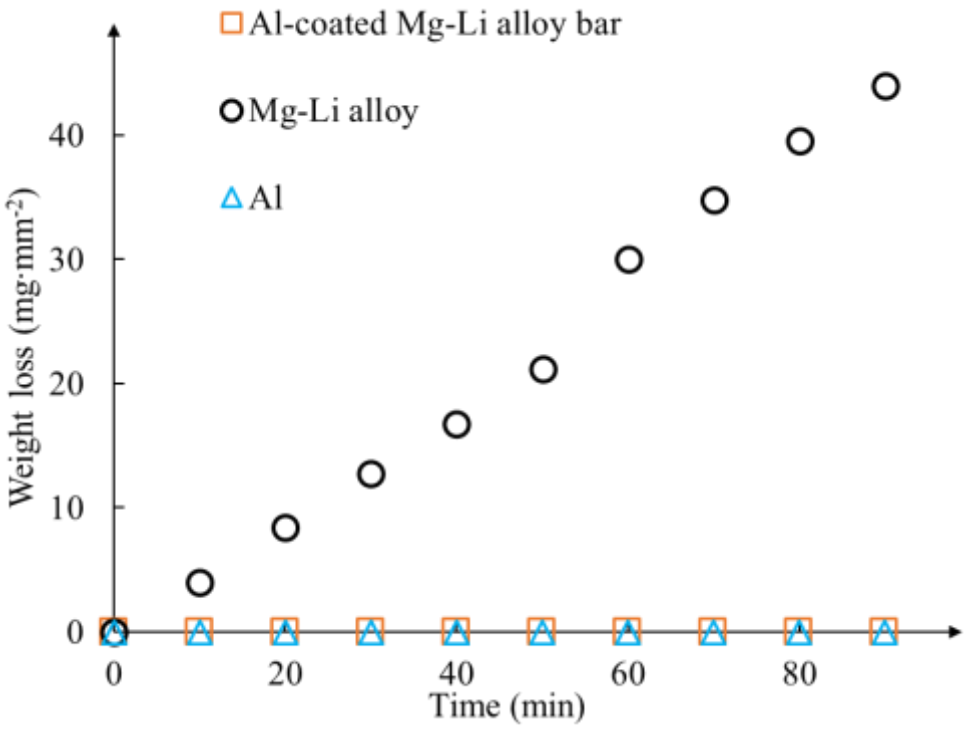

Fig. 2.8 Weight loss of different samples during immersion in a 0.5 mass% HCl aqueous solution.

2.4 Summary

In this chapter, the hot extrusion coating technique was demonstrated. By this method, the coating process was completed, and these conclusions listed below were obtained.

1. An Al-coated Mg-8Li alloy rectangular bar was successfully fabricated. A uniform and well bonded Al coating was produced with a thickness of approximately 200 μm.

2. The Al-coated Mg-8Li alloy bar exhibited excellent corrosion resistance in a 0.5 mass% HCl aqueous solution.

Chapter 3 Fabrication of Al coated Mg-Li alloy sheet by hot rolling

3.1 Introduction

In chapter 2, the Al-coated Mg-Li alloy bar was successfully fabricated by hot extrusion. However, in industry, bars have limited applications, and sheets are more widely used. Especially, for superplasticity forming, sheets are also necessary. Therefore, the feasibility of fabricating the Al-coated Mg-Li sheet from the as-extruded rectangular bar will be studied in this chapter. Rolling as the most general technique in industry will be used.

3.2 Experimental

The as-extruded Al-coated Mg-Li alloy rectangular bar produced in chapter 2 was used in this chapter. The bar was cut into small parts with a length of 30 mm in the extrusion direction. The small parts were rolled from 8 to 1.5 mm in thickness by 1 pass at 523 K using a two-high mill as shown in Fig. 3.1. The rolling direction was parallel to the extrusion direction. The microstructure was observed by using OM. To distinguish α phase and β phase in the Mg-Li alloy substrate, some samples were etched with a mixture of picric acid of 32 mL, acetic acid of 20 mL, distilled water of 20 mL, and ethyl alcohol of 18 mL before observation. The corrosion resistance was evaluated

by the same immersion test in a 0.5 mass% HCl aqueous solution as shown and introduced in Fig 2.4 in chapter 2.

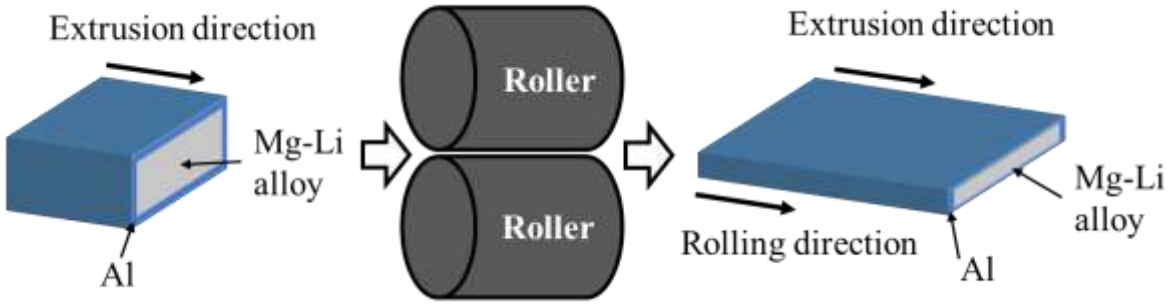

Fig. 3.1 Schematic illustration of the rolling process

3.3 Results and discussions

3.3.1 Microstructure of the Al-coated Mg-Li alloy sheet

Fig. 3.2 displays the appearance of the as-rolled Al-coated Mg-Li alloy sheet which has smooth surface and edges. Fig. 3.3 shows the microstructures of a longitudinal section of the sheet. The rolling direction corresponds to the traverse direction of the figures. The Al coating keeps uniform thickness in the rolling direction in Fig. 3.3 (a). In Fig 3.3 (b), the phases in the Mg-Li alloy substrate are elongated along the rolling direction, especially β phase (dark part in the Mg-Li alloy substrate in Fig. 3.3 (b)) is severely elongated because it is much more ductile than α phase (bright part in the Mg-Li alloy substrate in Fig. 3.3 (b)). Furthermore, cracks are not observed at the interface after the rolling deformation.

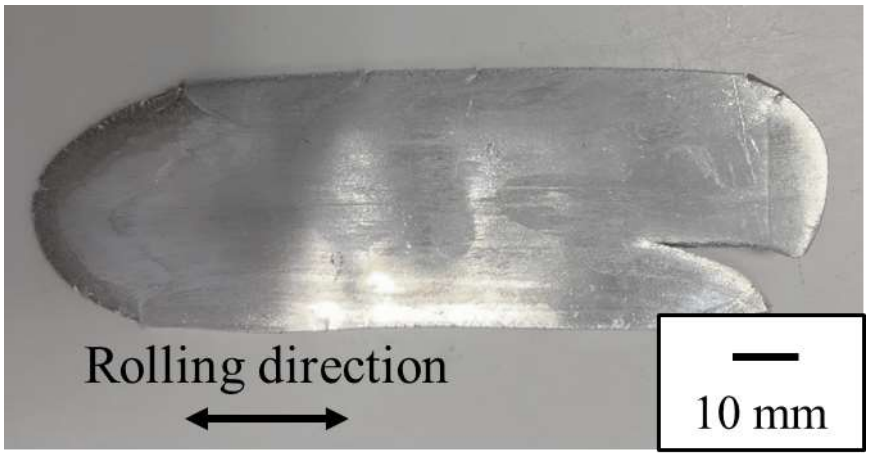

Fig. 3.2 Appearance of the as-rolled Al-coated Mg-Li alloy sheet

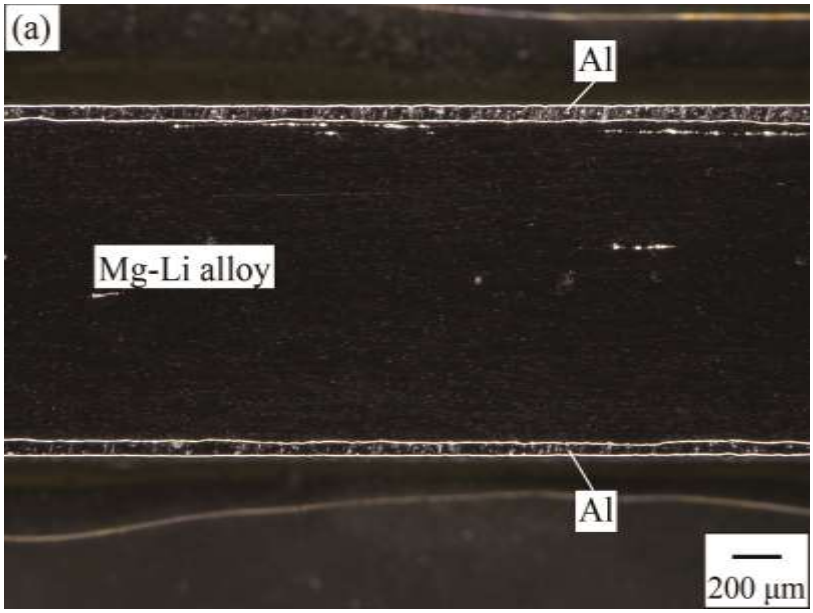

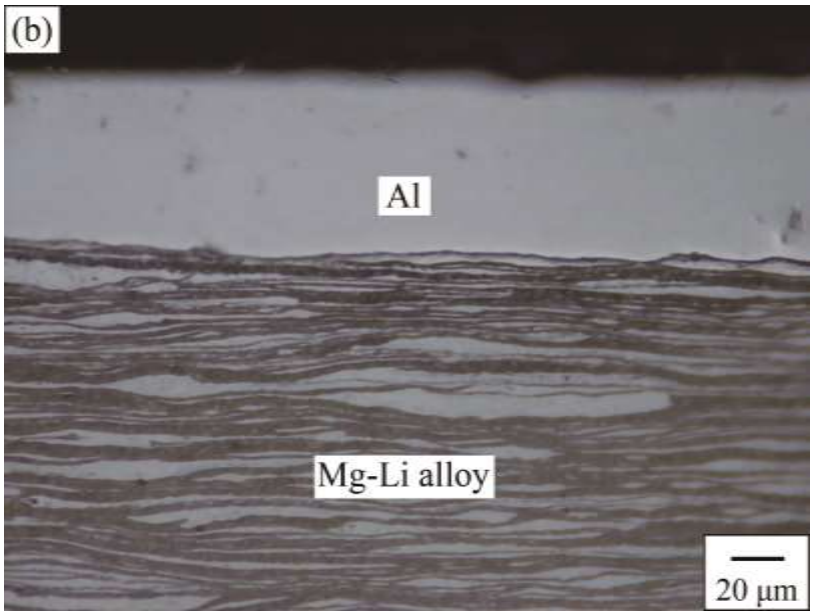

Fig. 3.3 (a) Longitudinal section of the as-rolled Al-coated Mg-Li alloy sheet, and (b) interface between Al coating and Mg-Li alloy substrate in the longitudinal section. The rolling direction corresponds to the traverse direction of the figures.

3.3.2 Corrosion resistance of the Al-coated Mg-Li alloy sheet

Fig. 3.4 displays the results of the immersion test of the as-rolled Al-coated Mg-Li alloy sheet in a 0.5 mass% HCl aqueous solution at room temperature. Without the Al coating, as marked by the circle, the Mg-Li alloy reacts with the acid solution seriously and loses its weight very quickly. However, the Al-coated Mg-Li alloy sheet sample has no weight loss in the HCl solution. Therefore, after the rolling deformation, the Al-coated Mg-Li alloy sheet keeps an excellent corrosion resistance.

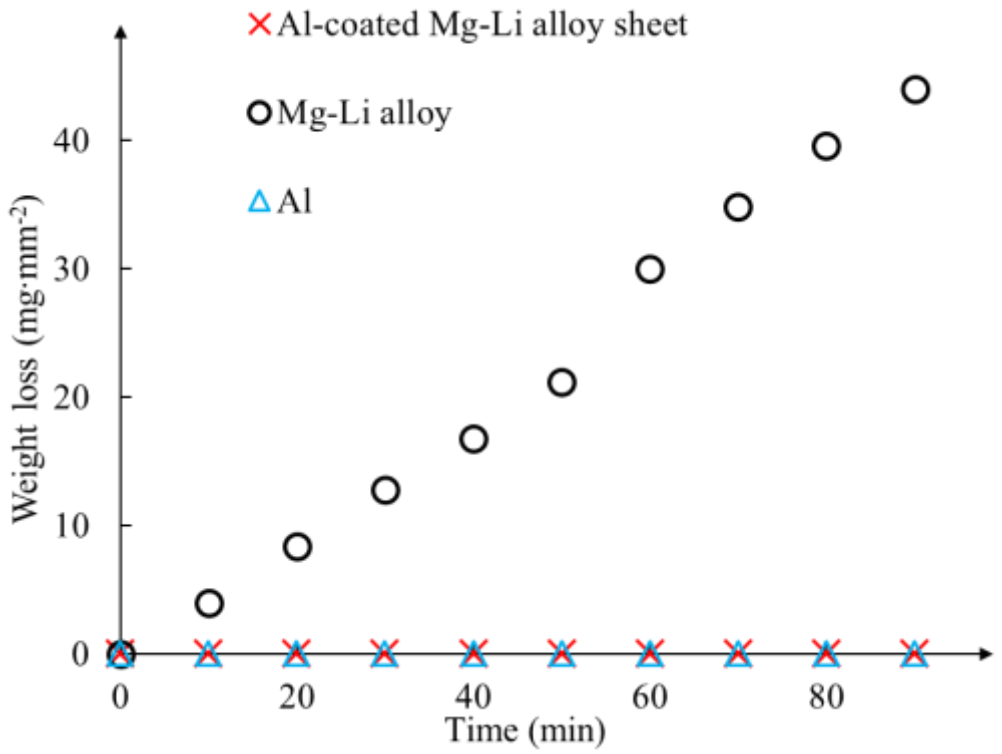

Fig. 3.4 Weight loss of different samples in a 0.5 mass% HCl aqueous solution.

3.4 Summary

In this chapter, the as-extruded Al-coated Mg-8Li alloy bar was deformed into sheet by hot rolling. After rolled into thin sheet, the coating kept uniform thickness and the bonding between the Al coating and Mg-Li alloy substrate remained good without forming any cracks at the bonding interface. The Al-coated Mg-Li alloy sheet also exhibited excellent corrosion resistance in a 0.5 mass% HCl aqueous solution.

Chapter 4 Tensile behavior of the Al-coated Mg-Li alloy sheet

4.1 Introduction

The Al-coated Mg-Li alloy sheet was successfully fabricated by hot rolling of the extruded rectangular bar, as described in chapter 3. The mechanical properties are of great importance to the formability of the sheet. Therefore, in this chapter, the tensile behavior of Al-coated Mg-Li sheet will be investigated.

4.2 Experimental

After the rolling process described in chapter 3, tensile specimens were cut from the as-rolled sheets by using a wire electrical discharge machine. The dimensions of the tensile specimen are shown in Fig. 4.1. The tensile direction is parallel to the rolling direction. Tensile tests were performed by an Instron tensile machine with a heating equipment. Room temperature tensile tests were conducted at room temperature at a strain rate of 0.001 s^{-1} in the air. Some specimens were heat treated at 573K for 60 mins before the tests. High temperature tensile tests were performed at temperatures ranging from 448 K to 573 K at stain rates of ranging from 0.001 s^{-1} to 0.01 s^{-1} both in the air and in an Ar atmosphere. Before every test, the specimen was set in the heater

equipped with the tensile machine and pre-heated for 10 mins at the test temperature before the tensile test.

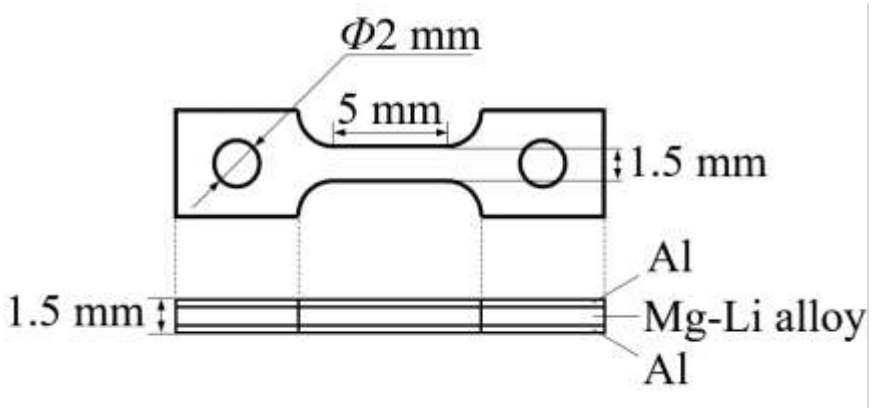

Fig. 4.1 Schematic drawings of the tensile test specimen; (a) top view and (b) longitudinal section.

Some microstructures of the specimens were observed by using OM. To distinguish between α phase and β phase in the Mg-Li alloy substrate, some samples were etched with a mixture of picric acid of 32 mL, acetic acid of 20 mL, distilled water of 20 mL, and ethyl alcohol of 18 mL before observation. The elements distribution and electron backscattering diffractions (EBSD) analyses were conducted by a JAMP-9500F Auger Electron Spectroscopy (AES). The fracture surfaces of the tensile specimens were observed by a JSM-6510LA Scanning Electron Microscope (SEM).

The corrosion resistance was evaluated by the same immersion test as that in chapters 2 and 3 in a 0.5 mass% HCl aqueous solution at room temperature. The sample for the corrosion test was prepared using a 150% elongated Al-coated Mg-Li alloy sheet, which was tensile-tested at 573 K at a stain rate of 0.001 s^{-1}.

4.3 Results and discussions

4.3.1 Room temperature tensile properties

Fig 4.2 shows the comparison of the room temperature tensile properties between Mg-Li alloy and pure Mg, which had the same deformation of extrusion and rolling described in chapters 2 and 3. By adding Li in Mg, the ductility can be largely improved from 10 to 35%. Fig 4.3 gives the stress-strain curves of the as-rolled Al-coated Mg-Li alloy sheets, exhibiting an ultimate tensile strength (UTS) of about 160 MPa and a fracture elongation of about 35% at room temperature. Therefore, the Al coating does not bring any bad influence on the fracture elongation of the Mg-Li alloy. Fig. 4.4 shows the longitudinal section of the fracture part of the tensile specimen, in which no cracks at the coating/substrate interface can be seen after the tensile elongation, which suggests that the deformation of the coating keeps good consistence with the deformation of the substrate. As more clearly shown in Fig. 4.4 (b), the coating finally exhibits a typical necking of a ductile material while the substrate exhibits a slight degree of necking associated with a shear fracture. In order to attempt to get a better plasticity, a heat treatment was performed. A heat treatment at 573 K for 60 minutes improved the fracture elongation to about 45% as illustrated by the red curve in Fig. 4.3, accompanied by a marked drop on the UTS.

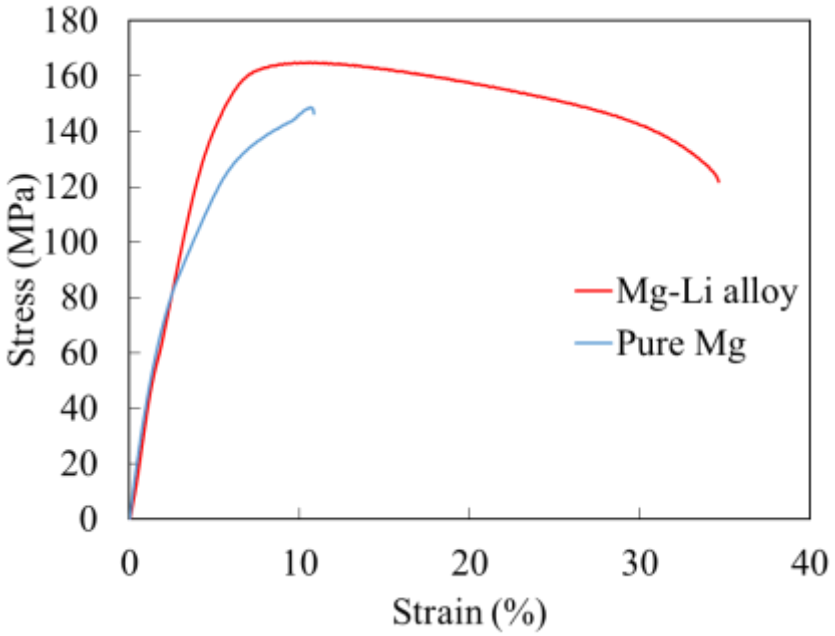

Fig. 4.2 Nominal stress-strain curves of Mg-Li alloy and pure Mg sheets at room temperature at 0.001 s^{-1}.

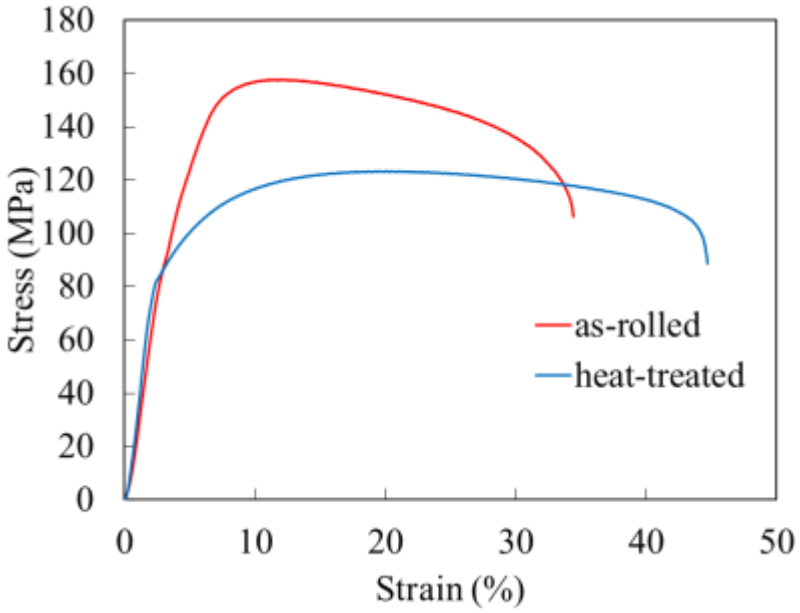

Fig. 4.3 Nominal stress-strain curves of the as-rolled and heat-treated Al-coated Mg-Li alloy sheets at room temperature at 0.001 s^{-1}.

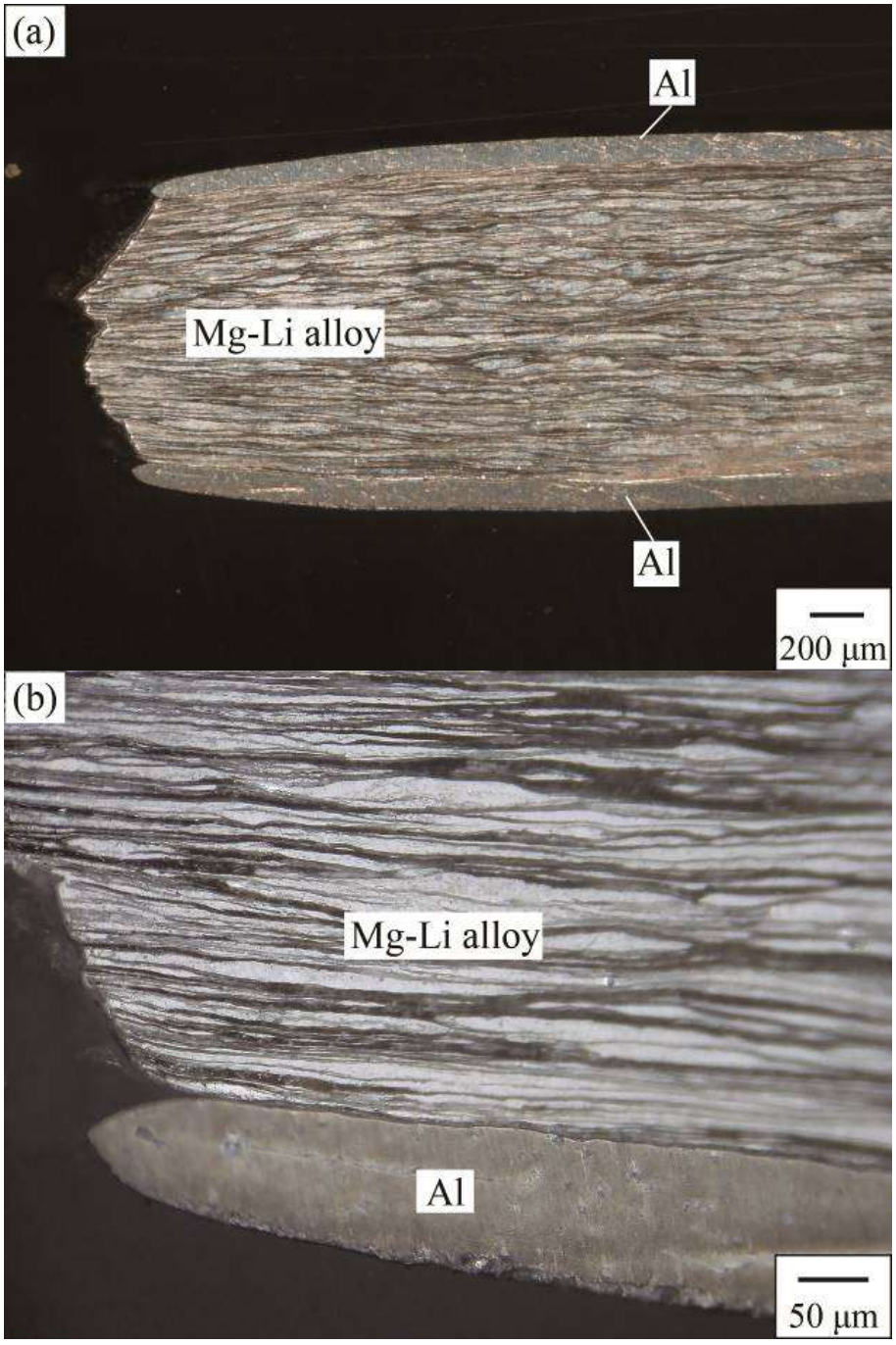

Fig.4.4 Longitudinal section of the as-rolled Al-coated Mg-Li alloy sheet elongated to fracture at room temperature; (a) low magnified image and (b) high magnified image of the Al coating part.

The growth of intermetallic compound (IMC) layer at the interface is an undesirable consequence after heating as shown in Fig. 4.5 (a), because IMCs are usually brittle and have bad influences on mechanical properties. Fig. 4.5 (b) is a line profile of the element distribution at the interface. Small platforms of the lines can be seen at the interface, suggesting the formation of the IMC. Notably, the diffusion of Li does not stop at the interface like Mg and Al. It has diffused far into the Al coating.

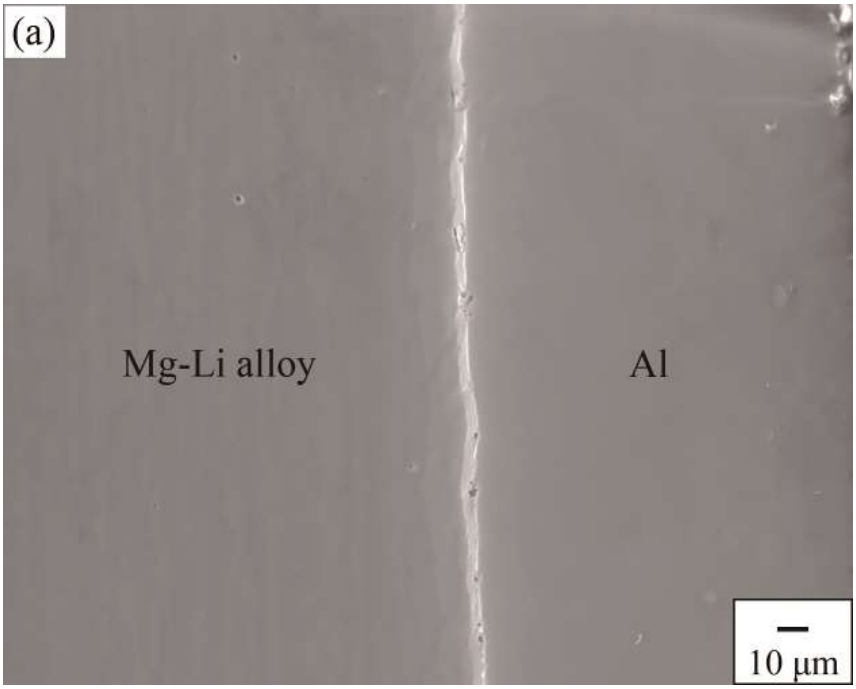

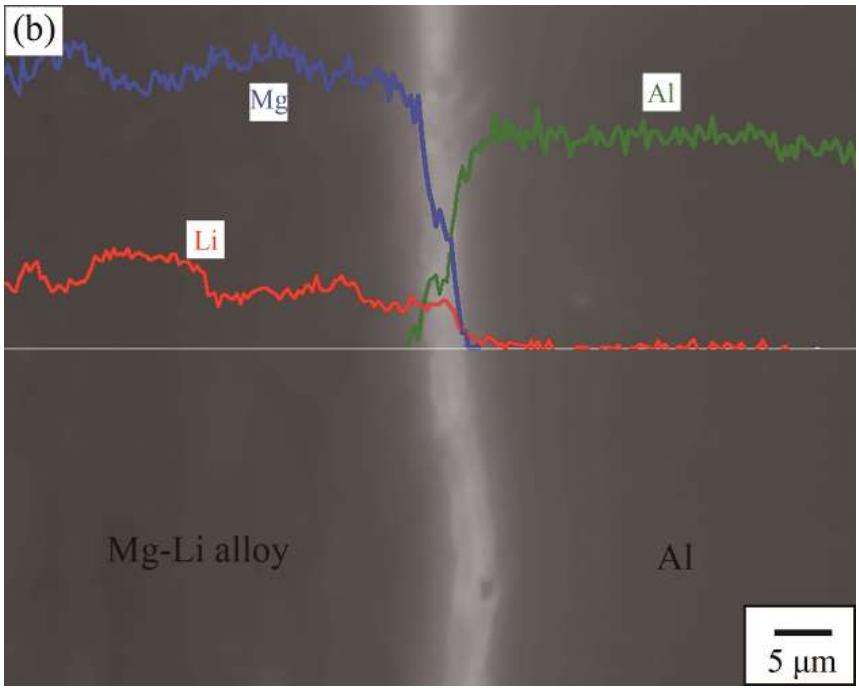

Fig. 4.5 (a) The SEM image of the intermetallic compound layer and (b) AES line profile showing the distribution of Li, Mg and Al at the Al/Mg-Li alloy interface after a heat treatment at 573 K for 60 minutes.

Fig. 4.6 shows the fracture surfaces of the specimens after tensile tests at room temperature. In Fig. 4.6 (a), without heat treatment, the Al coating has a sharp edge after fracture because of necking. And there is a smooth surface of the Al coating on the side close to the Mg-Li alloy. These are in agreement with the longitudinal section displayed in Fig. 4.4 (b). On the other hand, after a heat treatment at 573K for 60 minutes, the fracture surface of the Al coating becomes rough and exhibits a two-layered structure as shown in Fig. 4.6 (b), where the inner layer should be the IMC layer. The deep gap between the substrate and the coating suggests that the fracture may preferentially start from the IMC layer because of the low ductility of the IMC.

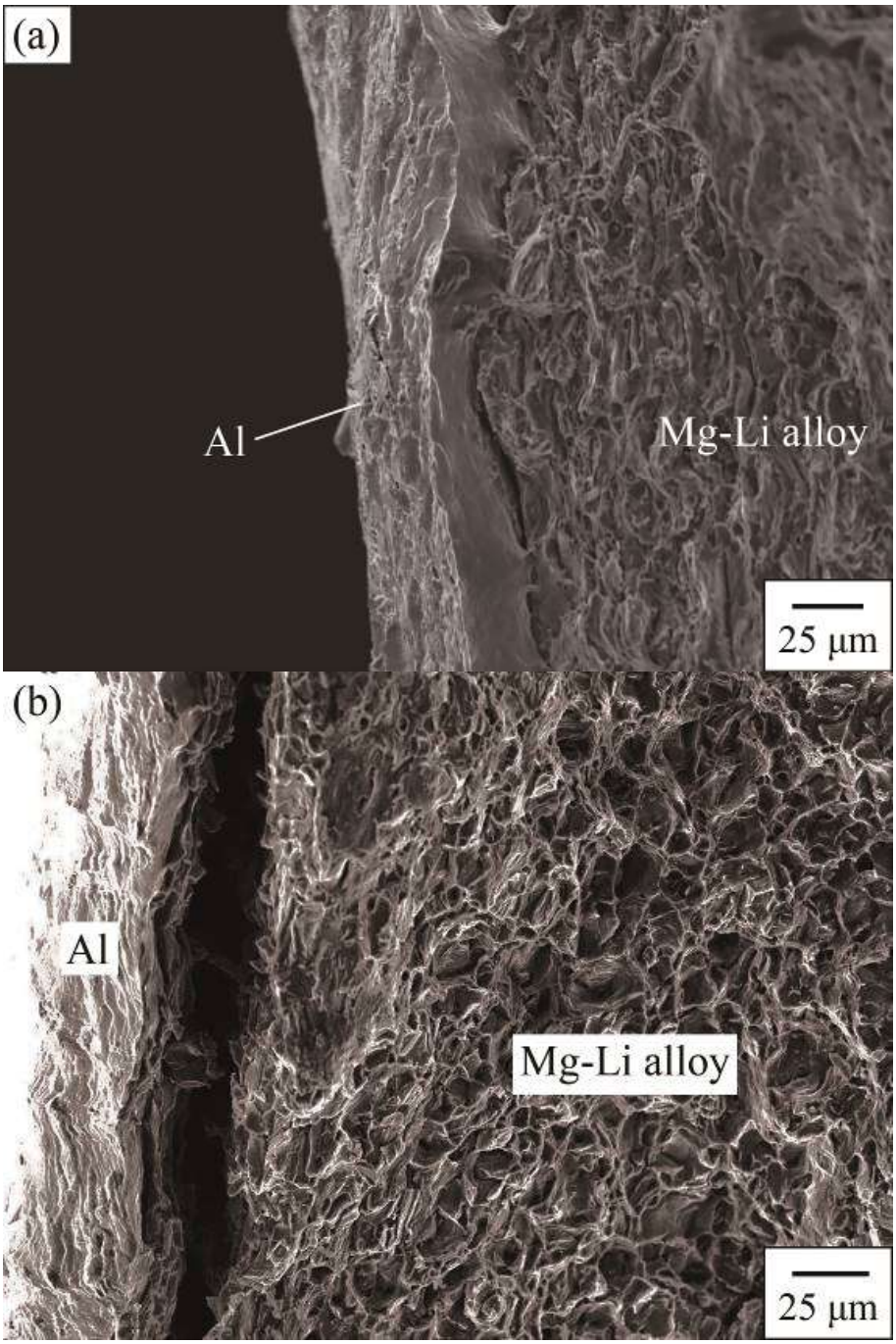

Fig. 4.6 SEM images of the tensile fracture surfaces of the specimens, (a) the as-rolled specimen without heat treatment and (b) the specimen after a heat treatment at 573 K for 60 mins.

4.3.2 High temperature tensile properties

Figs. 4.7 (a) and (b) illustrate the EBSD grain and phase image, respectively, of the as-rolled Al-coated Mg-Li alloy specimen just before the superplastic tensile test starting at 573 K, which is in fact a specimen after a heat treatment at 573 K for 10 mins according to the experimental procedures. In the grain map shown in Fig. 4.7 (a), in the Mg-Li alloy substrate, grains of both α and β phases are elongated along the rolling direction. The width of the elongated grain in the normal direction is less than 10 μm, while the lengths of many grains in the rolling direction are larger than 20 μm. This structure is not fine enough and not suitable for GBS. The grains of Al are equiaxed and most grains are less than 10 μm in size.

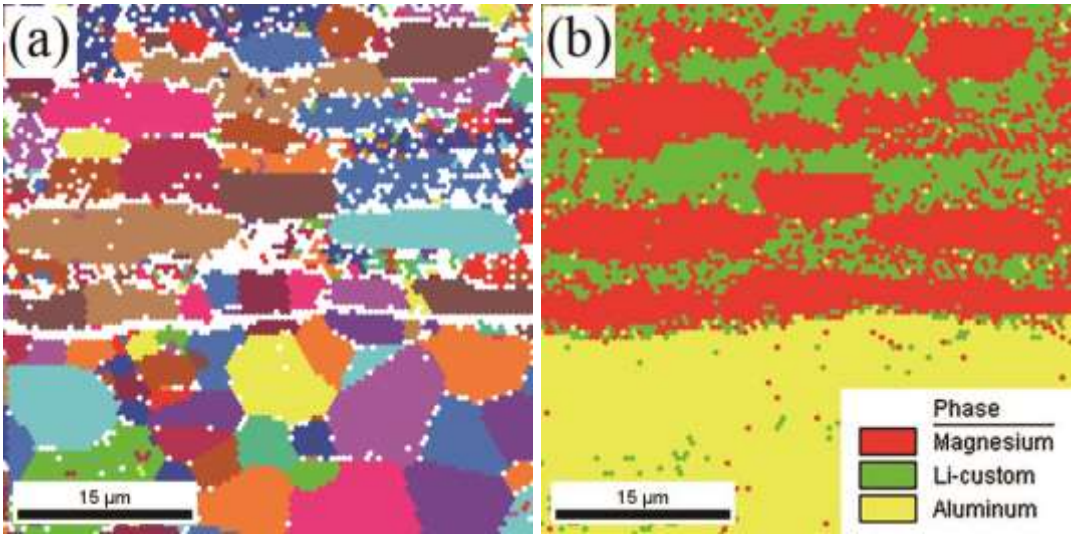

Fig. 4.7 EBSD image of the specimen before superplastic tensile test; (a) grain map and (b) phase map.

Fig. 4.8 (a) shows the stress-strain curves of the specimens tensile tested at different temperatures from 448 K to 573 K at 0.001 s^{-1}. At above 473 K,

the specimens can exhibit fracture elongations of about 200%, while at 448 K the fracture elongation decreases to about 170%. Additionally, as testing temperature rising, the flow stress falls dramatically. On the other hand, Fig. 4.8 (b) shows the stress-strain curves at the same temperatures at a higher strain rate of 0.01 s^{-1}. Compared with Fig. 4.8 (a), the flow stress is larger at the same temperature in Fig. 4.8 (b), while the fracture elongation decreases by about 50% at every temperature.

The shapes of the stress-strain curves imply a dynamic recrystallization (DRX) during the hot deformation process. The serrated curves in Fig. 4.8 (a) suggest discontinuous dynamic recrystallization (DDRX), which is usually observed in metals with low stacking fault energy, such as Mg [4.1]. In the hot deformation process, work hardening and softening by DRX influence the deformation behavior of the alloy. DDRX is usually a process of nucleation of new strain-free grains, which need an accumulation of dislocations to provide strain energy, which means there is a critical strain for it to start [4.2]. Therefore, on the stress -strain curve, the process of dislocation accumulation is the parts of hardening. After reaching the critical strain, nucleation of new strain-free grains occurs, and these grains grow at the expense of regions full of dislocations. The softening then can be seen on the stress-strain curve. Due to a low strain rate in Fig. 4.8 (a), dislocations accumulate slowly in this case. After the first DRX, the strain still cannot reach the critical strain for the second DRX to start. Therefore, the softening process ends, and another hardening process starts. Until the accumulation of dislocations in the new strain-free grains is enough for another DRX, the second DRX continues to begin to bring about another softening on the curve. And the hardening and

softening will occur alternatively to form the serrated curves. On the other hand, when at a high strain rate as showed in Fig. 4.8 (b), the accumulation of dislocations is very fast. In this case, after each DRX, it is fast to accumulate enough dislocation for the next DRX in the new strain-free grains. This means the work hardening and the softening by DRX take place simultaneously, but not alternatively. Therefore, serrated curves are not observed in this case.

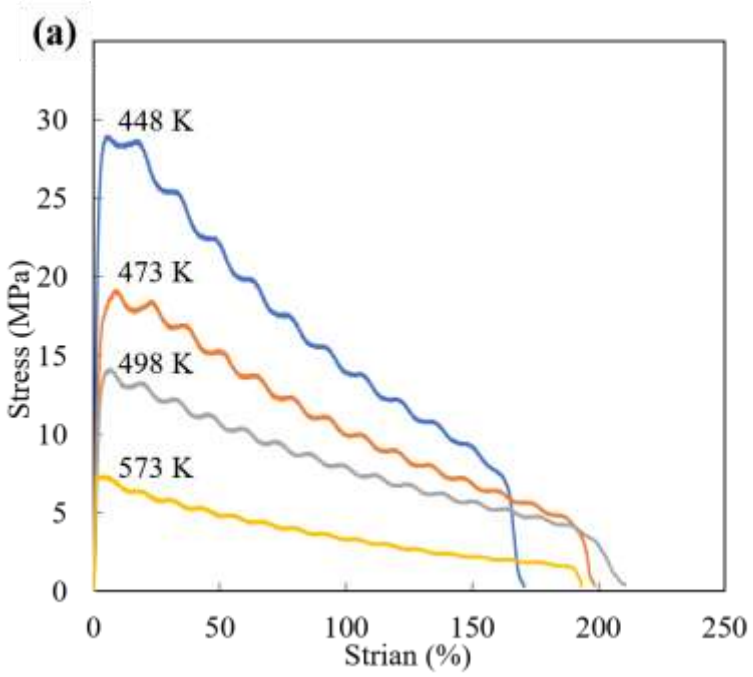

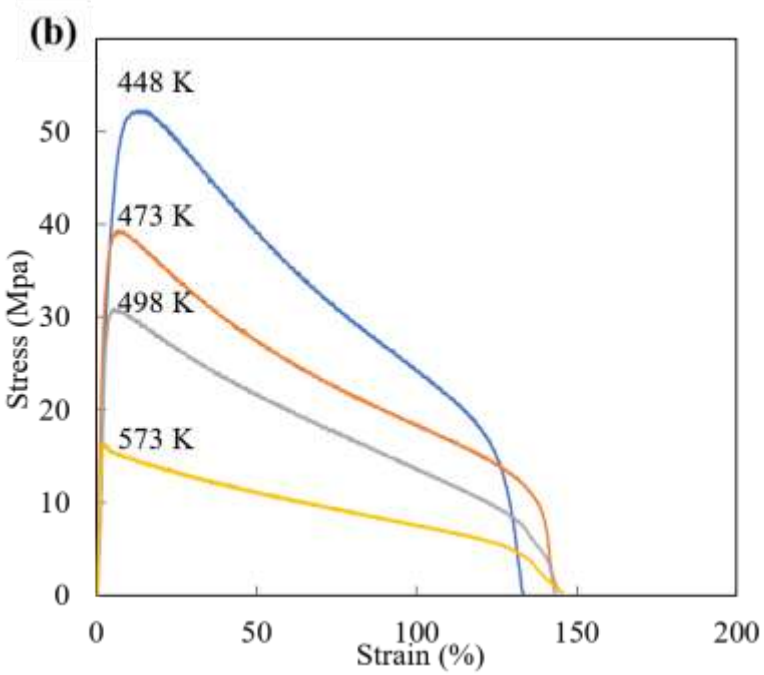

Fig. 4.8 Stress-strain curves of the specimens tensile tested at temperatures from 448 K to 573 K in the air at strain rates of (a) 0.001 s^{-1} and (b) 0.01 s^{-1}.

The superplastic deformation can be described by the following equation [4.3]:

$$\dot{\varepsilon} = \frac{ADG\boldsymbol{b}}{kT}\left(\frac{\boldsymbol{b}}{d}\right)^{p}\left(\frac{\sigma}{G}\right)^{n} \tag{4-1}$$

where $\dot{\varepsilon}$ is the strain rate, σ is the flow stress, D is the appropriate diffusion coefficient, G is the shear modulus, $\boldsymbol{b}$ is the Burgers vector, k is Boltzmann's constant, d is the grain size, T is the absolute temperature, p is the exponent of the grain size, n is the stress exponent and A is a dimensionless constant. The strain rate sensitivity index m ($m = \partial ln\sigma/(\partial ln\dot{\varepsilon}) = 1/n$) is important in describing the behavior of superplastic deformation. A large m value usually means more GBS and a large superplastic deformation. A typical superplastic deformation controlled by GBS is characterized by a m

value of about 0.5 [4.4-4.6]. The *m* values of the Al-coated Mg-Li alloy sheet at different temperatures are calculated as shown in Fig. 4.9. It is obvious that the *m* value increases as the temperature rises. The largest value is 0.38 at 573 K, which is quite smaller than 0.5. This means the amount of GBS in the deformation is not large enough, which is possibly because the coarse structure as stated above. Notably, the value of *m* falls greatly from 0.32 to 0.25 when temperature decreases from 473 K to 448 K. As shown in Fig. 4.7, fall of fracture elongation can be observed when temperature drops from 473 K to 448 K.

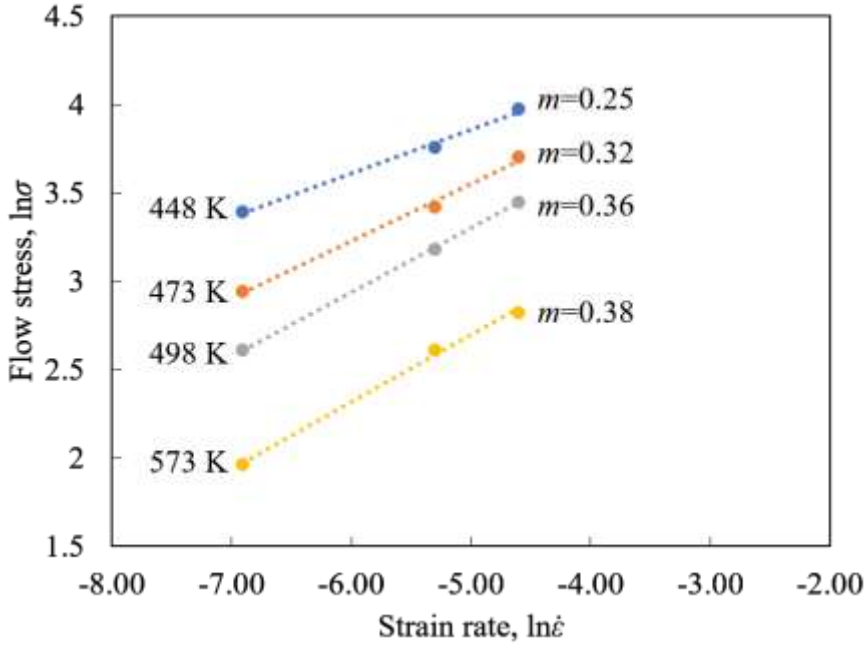

Fig. 4.9 Effects of strain rate on the flow stress of the Al-coated Mg-Li alloy sheet at different temperatures.

On the other hand, when the tensile test temperature is higher than 473 K, the fracture elongations are almost the same as seen in Fig. 4.8 (b), though the *m* value changes in Fig. 4.9. In fact, it was found that cracking always

occurred in the Al coating after the specimen was elongated to about 150%. Fig. 4.10 shows the longitudinal section of the specimen after an elongation of 150% at 573 K at 0.001 s^{-1}. Though the Al coating is unbroken, some small local necking can be seen. When the tensile elongation exceeded 150%, crack generation started on the Al coating, and consequently, the specimen fractured at an elongation of about 200% in the air, as shown in Fig.4.11. On the other hand, when tested in an Ar atmosphere, the fracture elongation increased and exceeded 400%, as shown on the bottom of Fig. 4.11. This is because that the overall elongation is limited by the Al coating. In fact, pure Al can exhibit an elongation of only 40% at 573 K at 0.001 s^{-1} [4.7], while the Mg-Li alloy without Al coating can be elongated to about 400% as show in Fig 4.12. If observed carefully in Fig. 4.11, there are many cracks on the Al coating of the specimen deformed in an Ar atmosphere. In contrast, the specimen deformed in the air has a small number of cracks only near the fracture part. The oxidation of the Mg-Li alloy during superplastic deformation in air at elevated temperatures has been reported in some researches [4.8]. In the case of this study, after a crack appears on the Al coating, the Mg-Li alloy substrate becomes exposed to the outside atmosphere. In the air, oxidation takes place and it should weaken the substrate where the crack generates and then causes a strain concentration there. Generally, the superplastic deformation mechanism has the ability to resist strain concentration. However, it has a limit, and the better superplasticity the larger limit. If the oxidation goes on to weaken the substrate too much and brings about too large strain concentration which exceeds the limit, a rapid fracture will occur near the crack. Differently, in an Ar atmosphere, the Mg-Li alloy substrate will not suffer from oxidation

even if the crack appears on the Al coating, which means that there is no that large strain concentration at the crack. Therefore, the specimen exhibits much larger elongation just as the original facture elongation as the Mg-Li alloy.

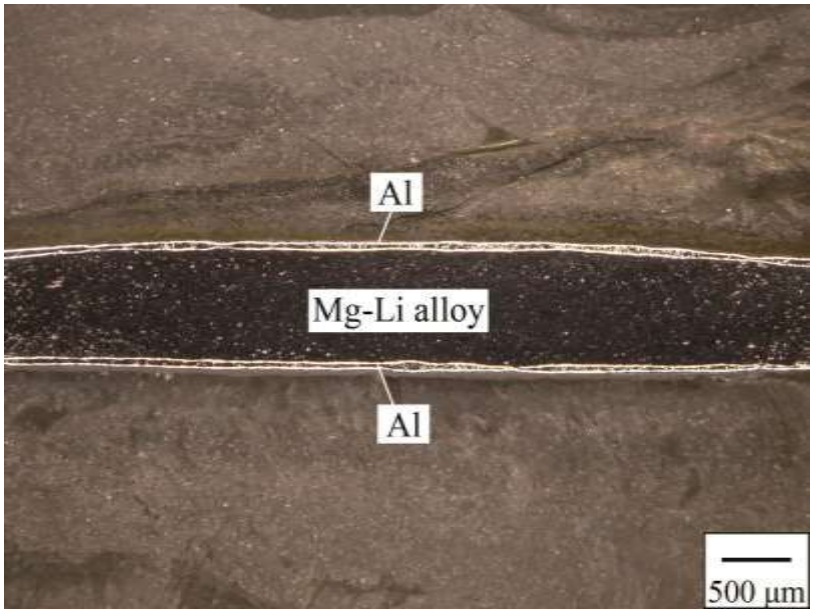

Fig.4.10 Longitudinal section of a tensile specimen of the Al-coated Mg-Li alloy sheet after a tensile elongation of 150% at 573 K at 0.001 s^{-1} in the air.

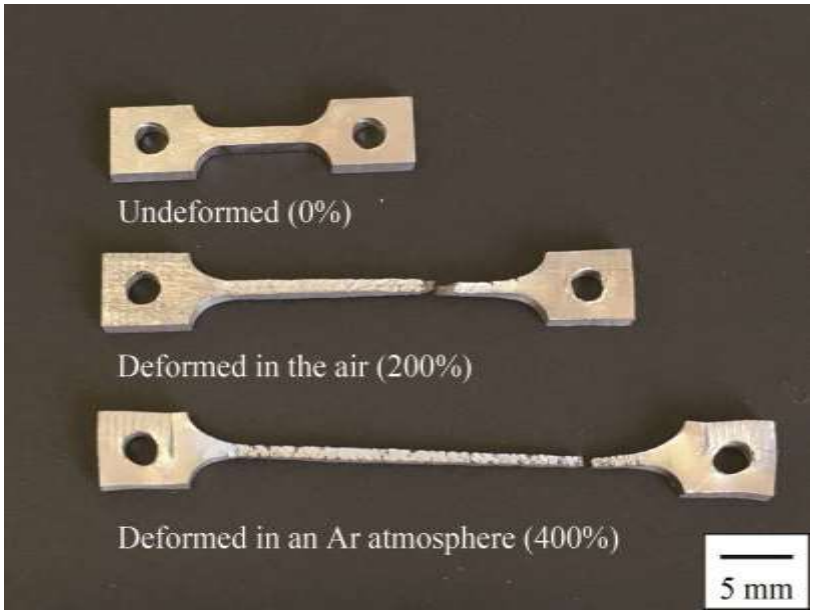

Fig. 4.11 Tensile specimens of the Al-coated Mg-Li alloy at 573 K at 0.001 s^{-1} in the air and in an Ar atmosphere.

Fig. 4.12 Tensile specimens of the Mg-Li alloy without Al coating at 573 K at 0.001 s^{-1} in the air.

4.3.3 Corrosion resistance of the tensile-elongated sheet

After a tensile elongation of 150% at 573 K at 0.001 s^{-1} in the air, the sheet still had an unbroken Al coating surface, as shown in Fig. 4.10. And then, the corrosion resistance of the elongated sheet was also checked by the immersion test. As shown in Fig. 4.13, the Al-coated Mg-Li alloy sheet elongated to 150% at 573 K at 0.001 s^{-1} also exhibits the same good corrosion resistance as the pure Al. This is because the Al coating exhibits a same elongation of 150% as the substrate. With the unbroken coating, the sheet can keep a good corrosion resistance even after a large elongation.

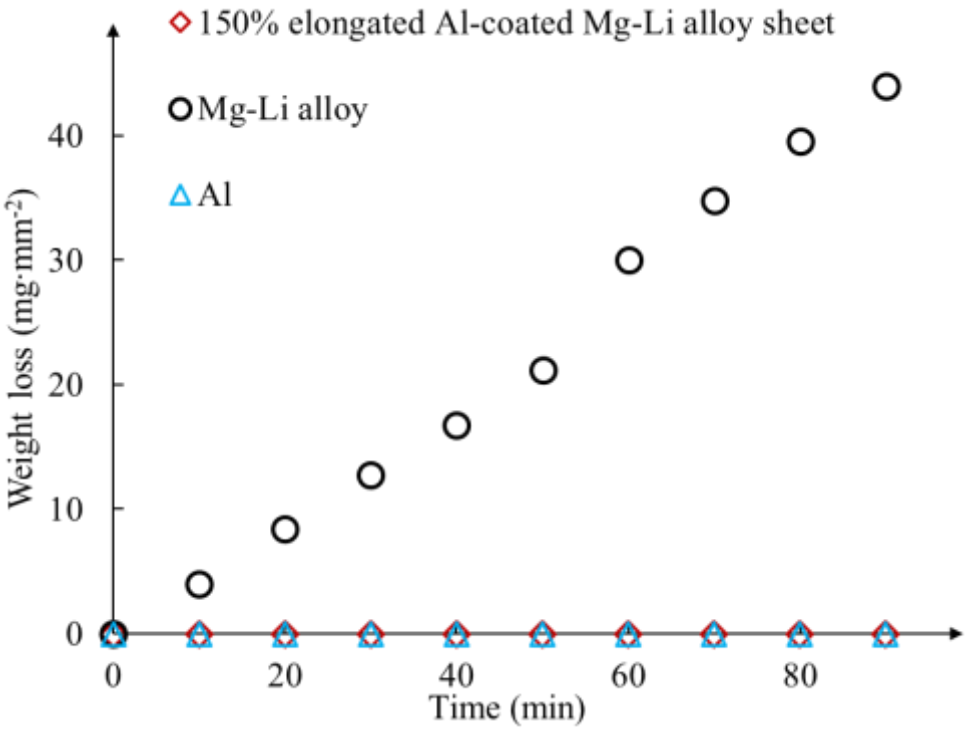

Fig. 4.13 Weight loss of different samples in 0.5 mass% HCl aqueous solution.

4.4 Summary

In this chapter, the tensile properties and corrosion resistance of the Al-coated Mg-8Li alloy sheet were investigated. Conclusions were obtained as below.

1. The as-rolled Al-coated Mg-8Li alloy sheet exhibited a fracture elongation of about 35% at room temperature at 0.001 s^{-1}. There is no break at the bonding between the substrate and coating.

2. The as-rolled Al-coated Mg-8Li alloy sheet exhibited fracture elongation of about 200% at 573 K at 0.001 s^{-1} in the air. The largest *m* value

was 0.38 at 573 K. The early fracture of Al coating and oxidation of the Mg-Li substrate restricted the overall elongation.

3. After an elongation of 150% in the air, the Al-coated Mg-Li alloy sheet still exhibited an excellent corrosion resistance in a 0.5 mass% HCl aqueous solution.

References

[4.1] K. Huang, R.E. Logé, A review of dynamic recrystallization phenomena in metallic materials, Mater. & Des. 111 (2016) 548-574.

[4.2] T. Sakai, J. J. Jonas, Dynamic recrystallization: Mechanical and microstructural considerations, Acta Metall. 32 (1984) 189–209.

[4.3] T. G. Langdon, The mechanical properties of superplastic materials, Metall. Trans. A 13 (1982) 689-701.

[4.4] P. Metenier, G. González-Doncel, O. A. Ruano, J. Wolfenstine, O. D. Sherby, Superplastic behavior of a fine-grained two-phase Mg-9wt.%Li alloy, Mater. Sci. Eng. A 125 (1990) 195-202.

[4.5] H. Somekawa, A. Kinoshita, K. Washio, A. Kato, Enhancement of room temperature stretch formability via grain boundary sliding in magnesium alloy, Mater. Sci. Eng. A 676 (2016) 427-433.

[4.6] H. Matsunoshita, K. Edalati, M. Furui, Z. Horita, Ultrafine-grained magnesium-lithium alloy processed by high-pressure torsion: Low-temperature superplasticity and potential for hydroforming, Mater. Sci. Eng. A 640 (2015) 443-448.

[4.7] T. Tokunaga, K. Matsuura, M. Ohno, Superplastic behavior of Al-coated Mg alloy sheet, J. Alloys Compd. 601 (2014) 179-185.

[4.8] X. H. Liu, H. B. Zhan, S. H. Gu, Z. K. Qu, R. Z. Wu, M. L. Zhang, Superplasticity in a two-phase Mg-8Li-2Zn alloy processed by two-pass extrusion, Mater. Sci. Eng. A, 528 (2011) 6157-6162.

Chapter 5 Effects of Zn addition on the tensile behavior of the Mg-Li alloy

5.1 Introduction

The Mg-8Li alloy was used in chapters 2, 3 and 4 as an example to introduce the fabrication and characteristics of the Al-coated Mg-Li alloy sheet. However, the comprehensive mechanical property of the Mg-8Li alloy was not high, especially its strength. To give more possible choices in practical application of the Mg-8Li alloy, Zn was added to the Mg-8Li alloy as an alloying element to improve the mechanical properties of the base Mg-Li alloy. The mechanical properties of 3 kinds of Al-coated Mg-Li alloy sheets using different base alloys: Mg-8Li (LZ80), Mg-8Li-2Zn (LZ82) and Mg-8Li-5Zn (LZ85) will be compared in this chapter.

5.2 Experimental

The fabrication processes of the Al-coated LZ82 and LZ85 alloy sheets were just the same as that of the LZ80 alloy as introduced in chapters 2 and 3. The method of the tensile test was also the same as that illustrated in chapter 4.

5.3 Results and discussions

5.3.1 Room temperature tensile properties

Fig. 5.1 shows the room temperature stress-strain curves of the Al-coated Mg-Li alloys with different levels of the Zn addition. Compared with the LZ80 alloy containing no Zn, the Al-coated LZ82 alloy has a small increase of ultimate strength (UTS) and a small increase of fracture elongation. Differently, the Al-coated LZ85 alloy exhibits a quite large improvement in UTS which is approaching 250 MPa, but a slight reduction in fracture elongation. Therefore, the small addition of Zn can improve both the strength and elongation. However, the larger addition of Zn reduces the fracture elongation, while it increases the tensile strength significantly. On the whole, both LZ82 and LZ85 alloys exhibits better comprehensive mechanical properties than the LZ80 alloy.

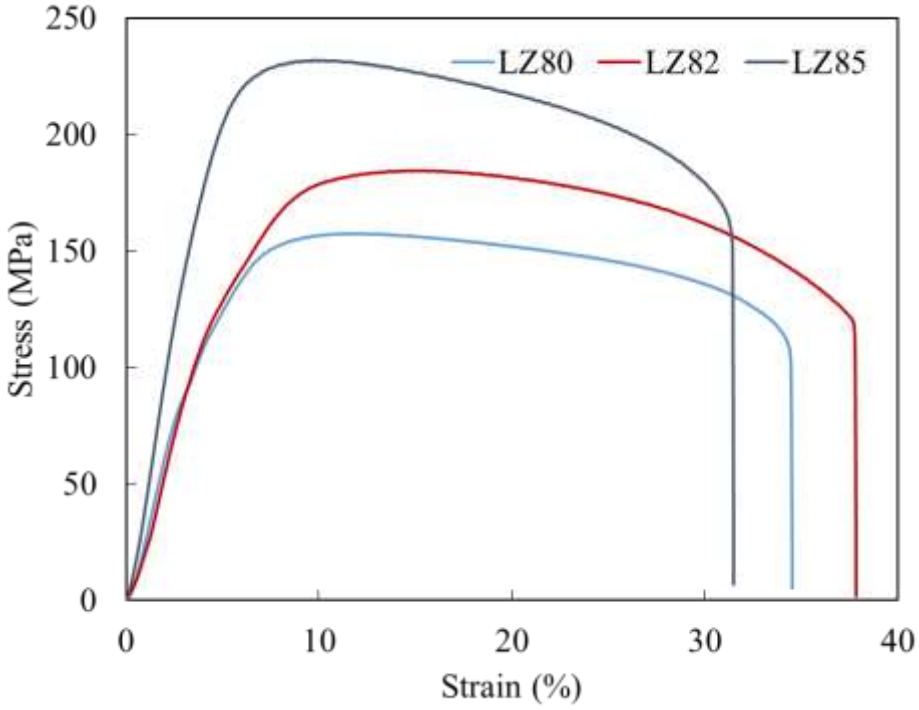

Fig. 5.1 Nominal stress-strain curves of the as-rolled Al-coated LZ80, LZ82 and LZ85 alloy sheets at room temperature at 0.001 s^{-1}.

5.3.2 High temperature tensile properties

Fig. 5.2 shows the stress-strain curves of the Al-coated LZ80, LZ82 and LZ85 alloys at 573K at 0.001 s^{-1}. The addition of Zn did not change the high temperature tensile properties largely. With the increase in Zn concentration, the fracture elongation has a slight increase form about 200% to about 250%. At the same time, the flow stress shows a small decrease. Though these changes brought about by the Zn addition have good influence on superplastic deformation, they are still far from an enough level. Therefore, the superplasticity cannot be improved largely only by the alloying of Zn.

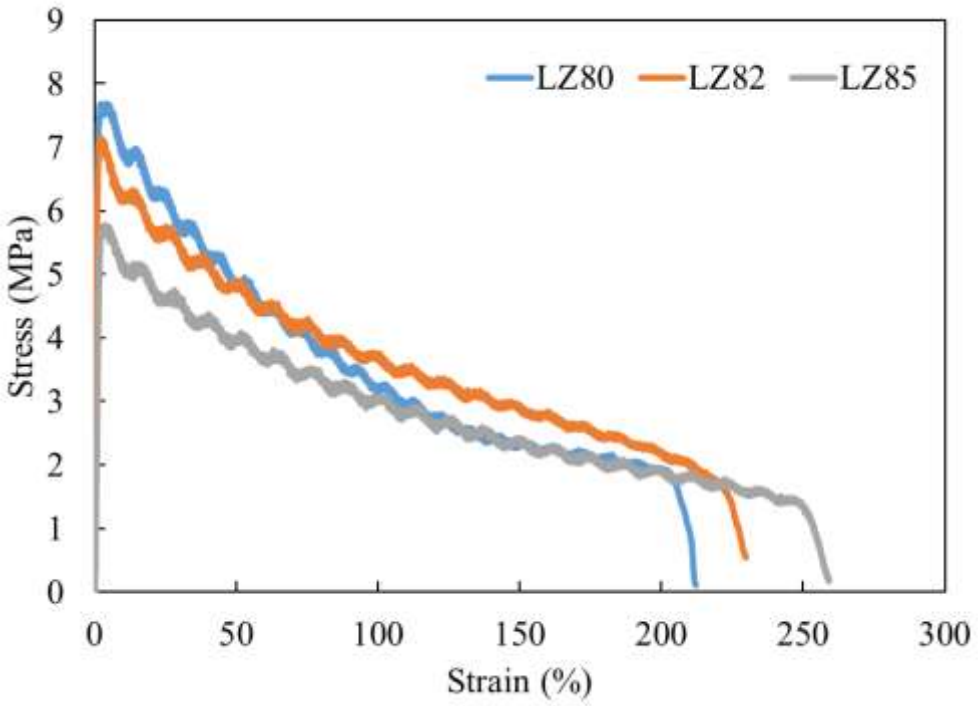

Fig. 5.2 Nominal stress-strain curves of the as-rolled Al-coated LZ80, LZ82 and LZ85 alloy sheets at 573K at 0.001 s^{-1}.

5.4 Summary

In this chapter, the tensile properties of the Al-coated LZ82 and LZ85 alloy sheets were investigated, which are produced and tested by the same methods as demonstrated in chapters 2, 3 and 4. The addition of Zn brought about improvements of room temperature tensile properties, especially a large improvement of strength was observed with the use of LZ85 alloy. However, no large improvement of the superplasticity was observed in the high temperature tensile tests. Therefore, the alloying with Zn cannot effectively improve the superplasticity of the Mg-Li alloys. The refinement of structure

by much larger plastic deformation is still the key point to achieve a good superplasticity, which will be discussed in the next chapter.

Chapter 6 Structure refinement and improvement of superplasticity by multi extrusion-rolling process

6.1 Introduction

Though the Al-coated Mg-Li alloy sheets were successfully fabricated as described in the past chapters, the extrusion and rolling during the processing could not give adequate plastic deformation to produce a fine enough structure. Therefore, in this chapter, a special deformation process will be developed to refine the structure of the Mg-Li alloy. The LZ85 alloy is used as the base alloy because of its good comprehensive mechanical properties as illustrated in chapter 5.

6.2 Experimental

The procedure of the multi extrusion-rolling process used in this study is shown in Fig. 6.1. A Mg-8 wt% Li-5 wt% Zn (LZ85) alloy was used. First, using the similar method described in chapters 2 and 3, the ingot was extruded into a rectangular bar at 473 K with a reduction of 90%, and consequently rolled into 2 mm thick sheets at 473 K with a reduction of 75% in 1 pass. Secondly, these sheets after one pass of extrusion and one pass of rolling (noted as ER samples) were stacked in the container set as a billet for the

second extrusion process, which is shown at the start in Fig. 6.1. A rectangular die was put on the top of the stacked sheets and rams were set upon the die. The size and shape of the die are shown in Fig. 6.2. After this setting, the container was heated from room temperature to 473 K and then the extrusion was carried out under a pressure of 250 MPa at a ram speed of 0.6 mm/s. By this extrusion, a rectangular bar was produced. Finally, this bar was consequently rolled from 8 mm to 1.5 mm in thickness at 473 K by a two-high mill in 1 pass. This new as-rolled sheet is noted as ERER sample. In the second extrusion process, by putting an Al plate on the top of the Mg-Li alloy sheets, an Al coating can also be given on the subsequent bar as that in chapter 2. Then after rolling, the Al-coated ERER sheet can be produced. The rolling direction was always parallel to the extrusion direction before the present rolling process. Tensile specimens were cut from the sheets by a wire electrical discharge machine. The tensile tests were performed by the same method as that described in chapter 4. The tensile direction was parallel to the rolling direction. The tensile tests were performed at 423 and 473 K at three different stain rates of 0.001, 0.005 and 0.01 s^{-1} in air.

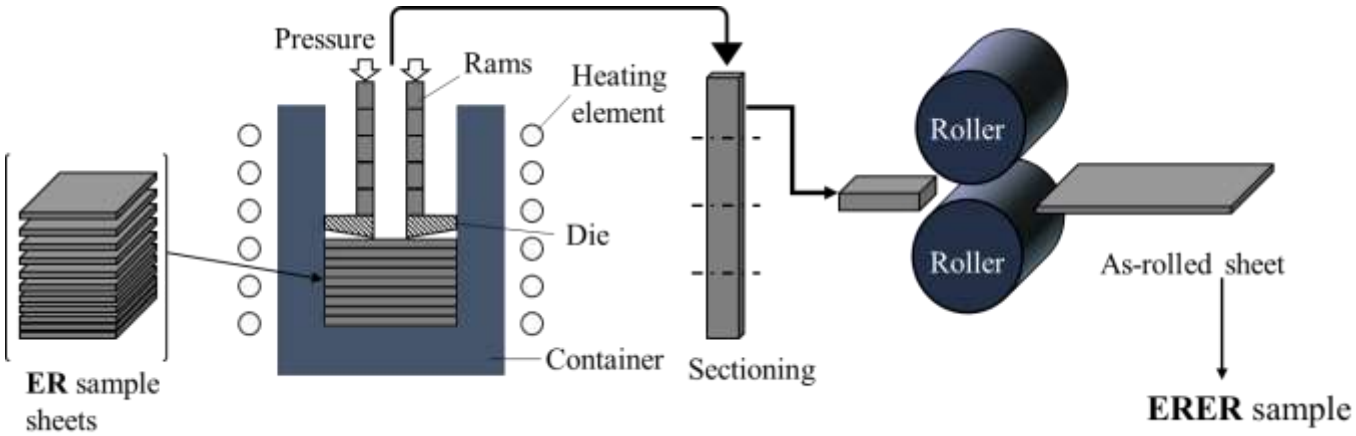

Fig. 6.1 Schematic drawing of the multi extrusion-rolling process

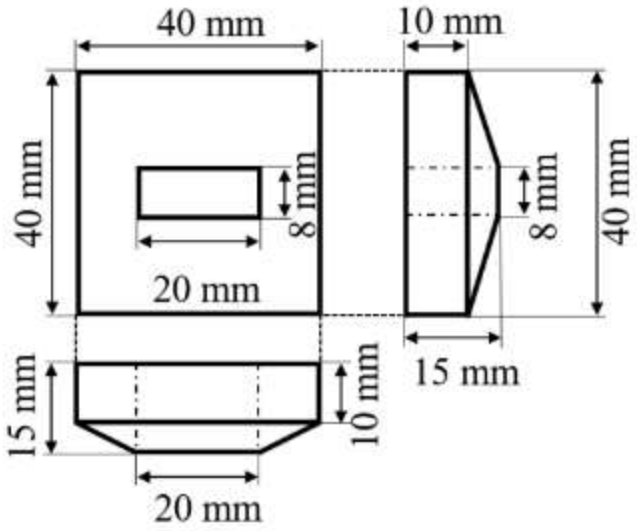

Fig. 6.2 Schematic drawing of the die.

The microstructures of the samples were observed by OM. To distinguish between α and β phases in the Mg-Li-Zn alloy, some samples were etched with a mixture of picric acid of 32 mL, acetic acid of 20 mL, distilled water of 20 mL and ethyl alcohol of 18 mL before observation. Scanning electron micrographs (SEM), inverse pole figures (IPF) and pole figures (PF) were obtained by a JAMP-9500F Auger Electron Spectroscopy (AES) equipped with an electron backscatter diffraction (EBSD) device.

6.3 Results and discussions.

6.3.1 Refinement of the microstructure of the Mg-Li alloy

Figs. 6.3 (a) and (b) show the microstructures of the ER samples, where the bright area is α phase (Mg-rich, HCP) and the dark area is β phase (Li-rich, BCC). In Fig. 6.3 (a), which shows the rolling plane, both α and β phases are elongated along the rolling direction (RD). In the normal direction (ND) they form a lamellar structure. Some coarse parts of α phase can be observed. In Fig. 6.3 (b), which shows the RD/transverse direction (TD) plane, the two phases are both in very coarse size and exhibit irregular shapes. Thus, it is difficult to produce a fine microstructure in the LZ85 alloy only by one pass of ordinary extrusion and rolling. However, in the ERER sample after the subsequent special extrusion process and rolling, the microstructures become much finer than the ER samples, as shown in Figs. 6.3 (c) and (d). Especially, by comparing Figs. 6.3 (d) with (b), it is clearly shown that the coarse grains have almost disappeared, and a significant refinement has been achieved.

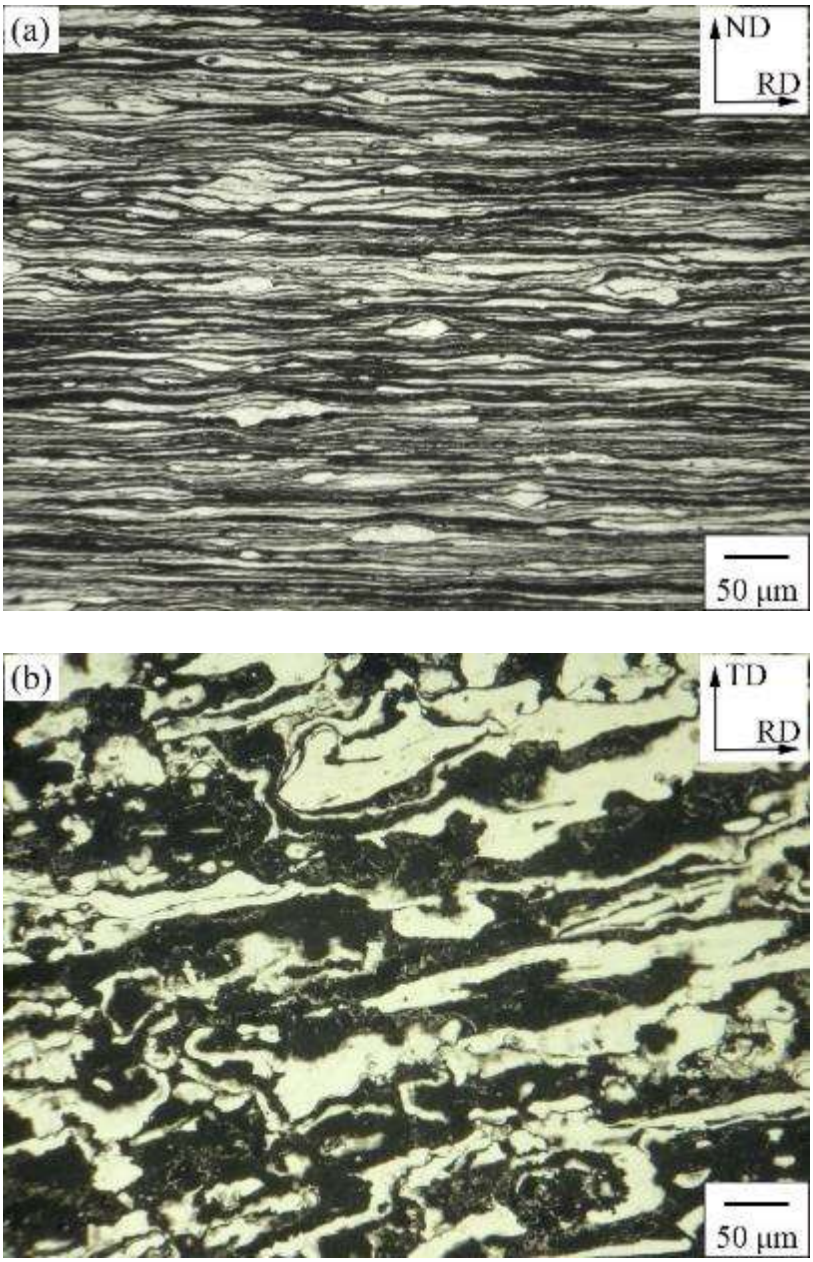
(a)
ND
RD
50 μm
(b)
TD
RD
50 μm

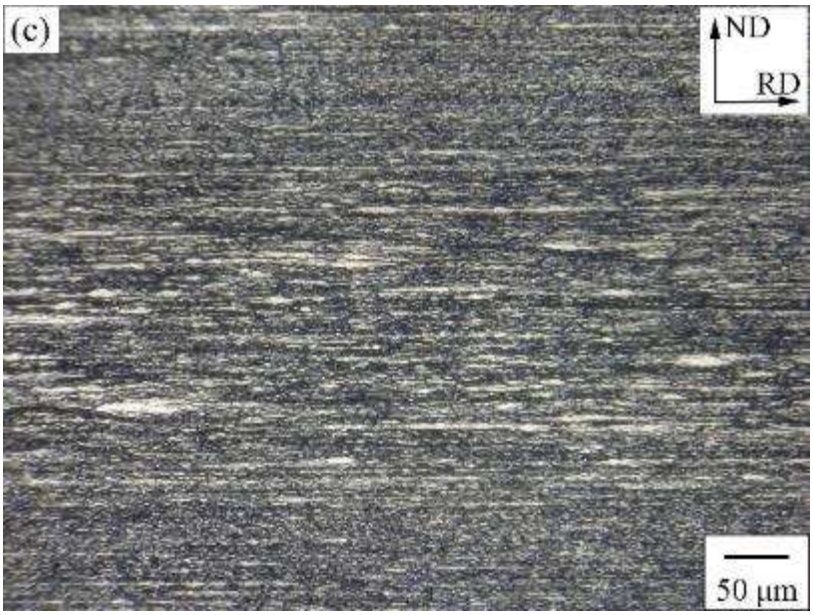
(c)
ND
RD
50 μm

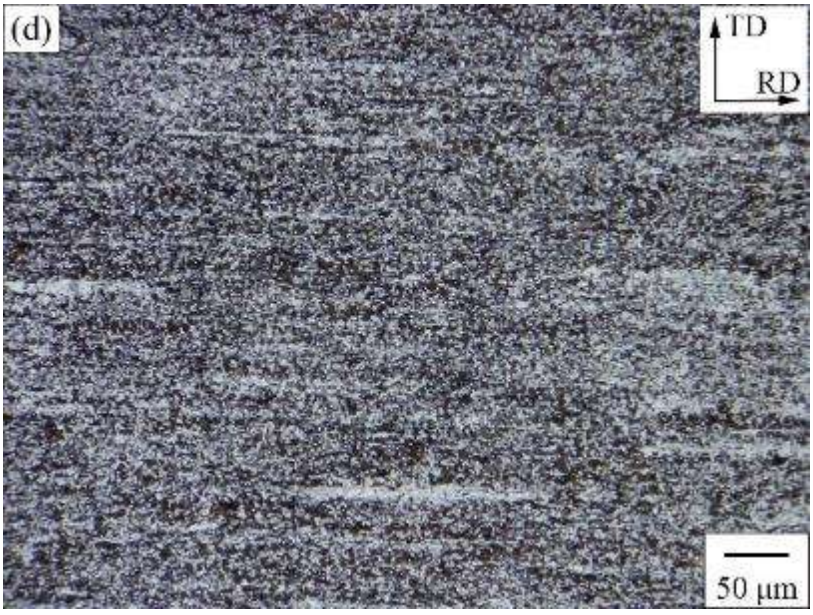
(d)
TD
RD
50 μm

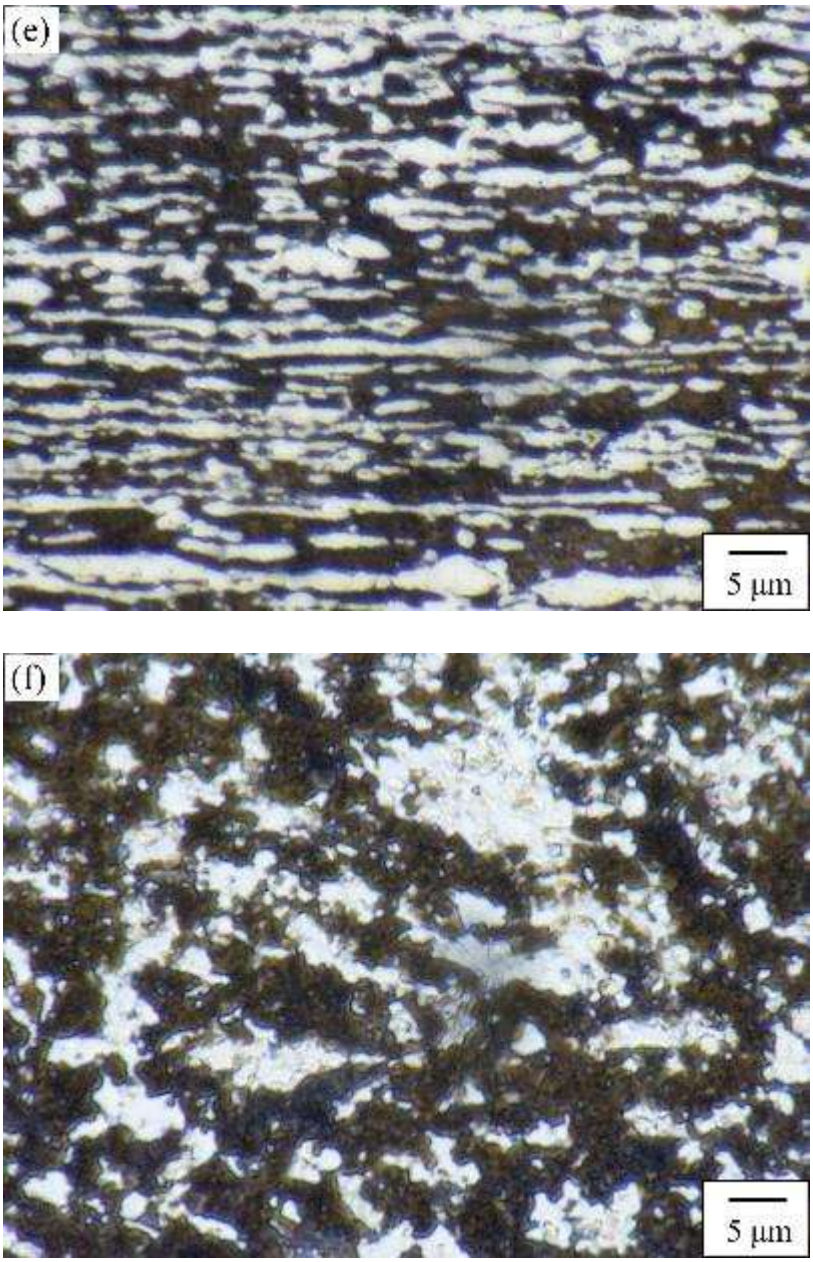

Fig. 6.3 Microstructures of the rolled samples on different cutting planes, (a) and (b) the ER samples, (c) and (d) the ERER samples, (e) and (f) the enlarged pictures of (c) and (d).

6.3.2 High temperature tensile properties

6.3.2.1 High temperature tensile properties of the ERER specimens

Fig. 6.4 shows the stress-strain curves of the ERER specimens tested in tension at 473 and 423 K at various strain rates, and Fig. 6.5 shows the appearances of the corresponding specimens after tensile tests. At 473 K the specimen exhibits a large elongation of about 1400% at a moderate strain rate of 0.001 s^{-1} as shown in Fig. 6.4 (a). Even at a higher strain rate of 0.01 s^{-1}, the specimen can be elongated to over 600% without any obvious necking, which implies a high-strain-rate superplasticity. On the other hand, in Fig. 6.4 (b), at a lower temperature of 423 K, the specimen still exhibits a quite high superplastic elongation of over 700% at 0.001 s^{-1}. However, at a high strain of 0.01 s^{-1}, the elongation drops to 250% with obvious necking which can be observed in Fig. 6.5 (b). Compared with the results without the multi extrusion-rolling process described in chapter 4, not only the fracture elongation was largely improved, but more importantly, the large superplastic elongation can be achieved at lower temperatures and higher strain rates. This can bring many practical benefits for SPF, for superplasticity at low temperatures and at relatively high strain rates can lower the production cost and shorten the production time.

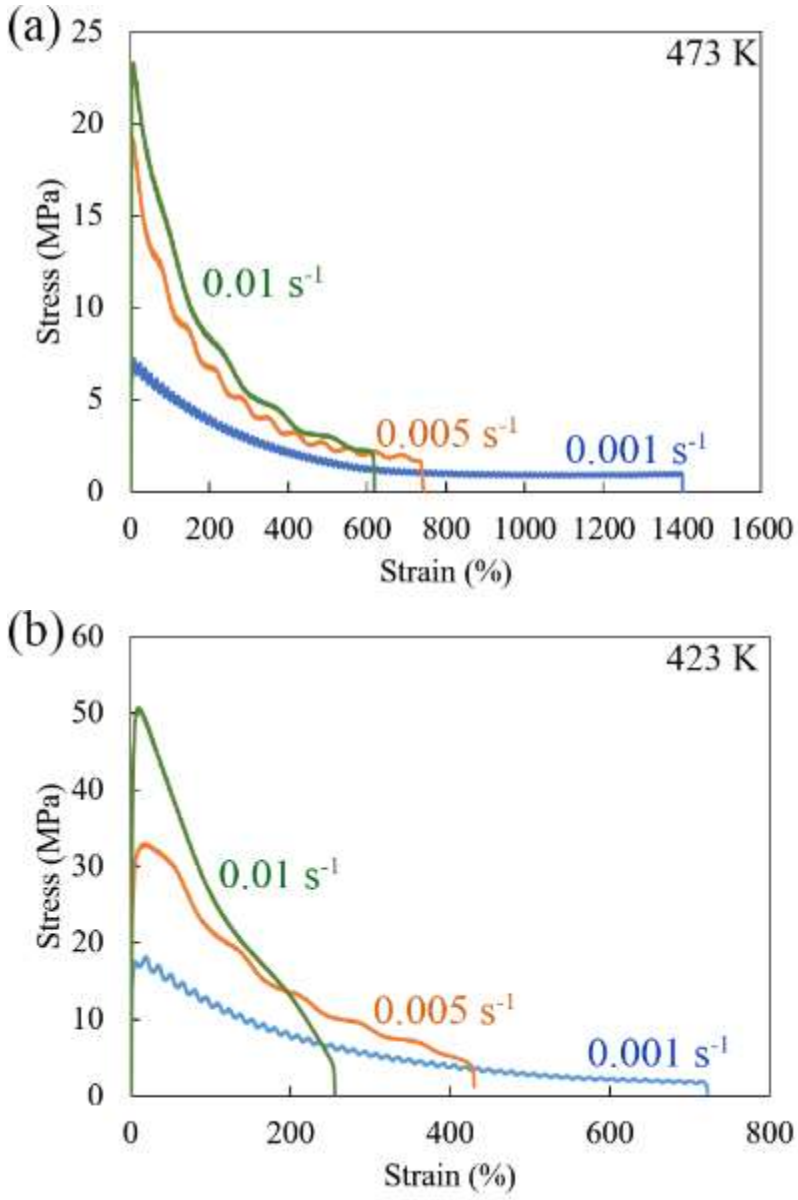

Fig. 6.4 Engineering stress-strain curves of the ERER specimens tested in tension at 0.001, 0.005 and 0.01 s^{-1} at (a) 473 K and (b) 423 K

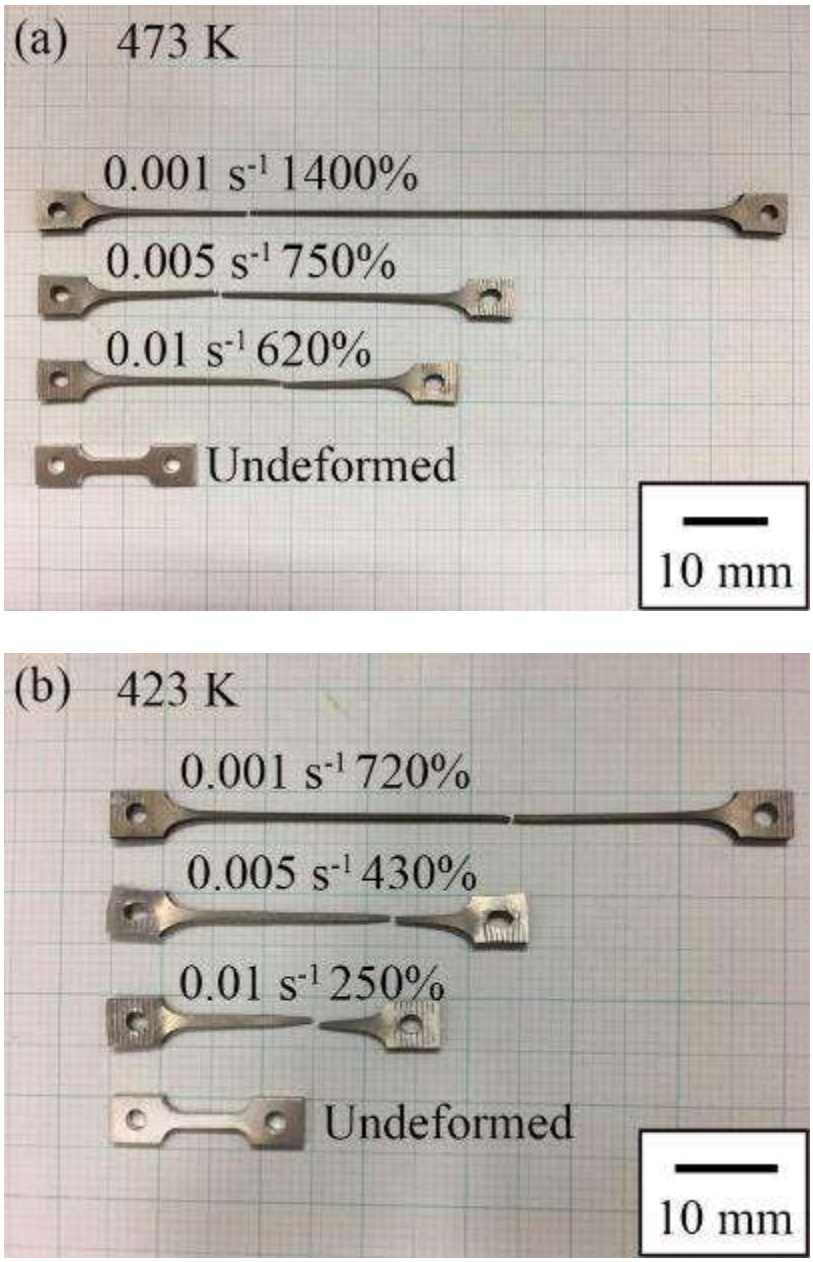

Fig. 6.5 Appearances of ERER specimens after tensile tests at 0.001, 0.005 and 0.01 s^{-1} at (a) 473 K and (b) 423 K.

6.3.2.2 High temperature tensile properties of the Al-coated ERER specimens

Fig. 6.6 shows the stress-strain curves of the Al-coated ERER specimens tested in tension at 473 K and 423 K at various strain rates, and Fig. 6.7 shows the appearances of the corresponding specimens after tensile tests. Attributing to large improvements of superplasticity of the base Mg-Li alloy, the fracture elongations of the Al-coated specimens also exhibit large increases, compared with the specimens without the multi extrusion-rolling deformation process. At 473 K the specimen exhibits an elongation of about 900% at 0.001 s^{-1} as shown in Fig. 6.6 (a). However, in Fig. 6.7 (a), cracks can be observed on the Al coating. At a higher strain rate of 0.005 s^{-1}, the specimen can be elongated to about 400% without any cracks on the Al coating. At 423 K, the specimens were also elongated to about 400% without cracks. Overall, after the multi extrusion-rolling process, the crack-free elongation of the Al-coated specimen has also been largely improved. Notably, these can be achieved at lower temperatures and higher strain rates. Consequently, another benefit, as show in Fig. 6.8, is the formation of the IMC can be suppressed due to low temperature and less heating time.

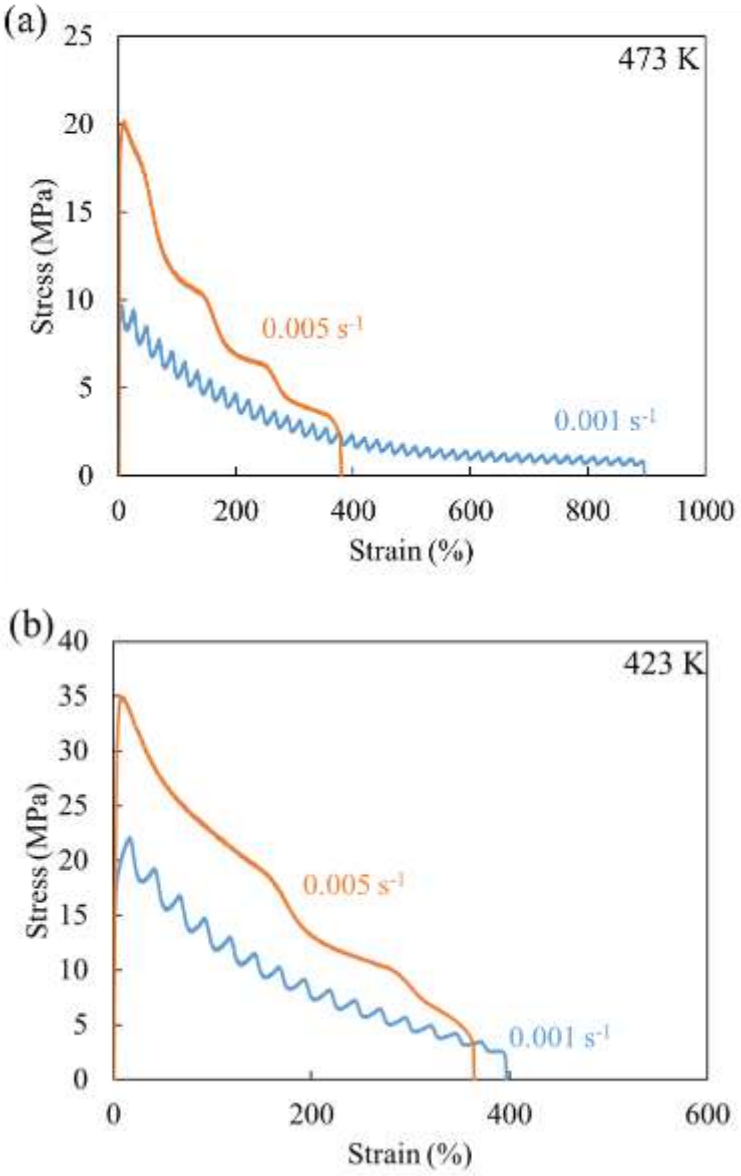

Fig. 6.6 Engineering stress-strain curves of the Al-coated ERER specimens tested in tension at 0.001 and 0.005 s^{-1} at (a) 473 K and (b) 423 K.

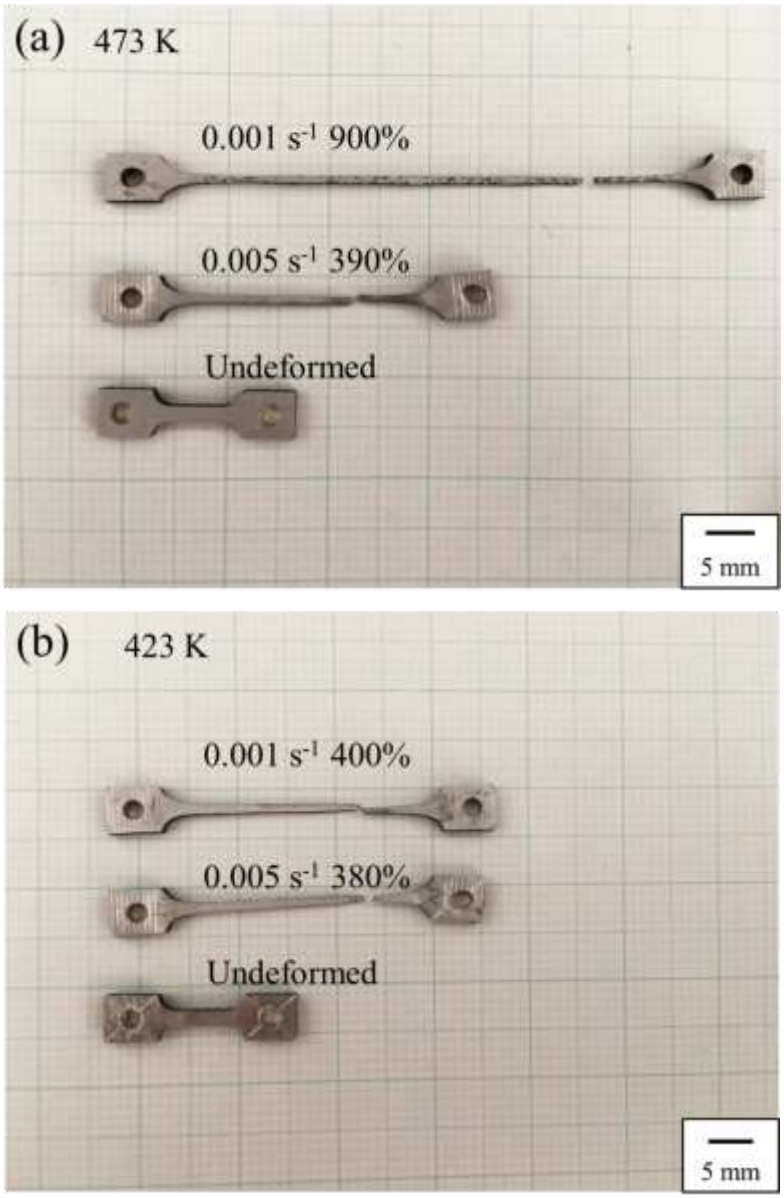

Fig. 6.7 Appearances of Al-coated ERER specimens after tensile tests at 0.001 and 0.005 s^{-1} at (a) 473 K and (b) 423 K.

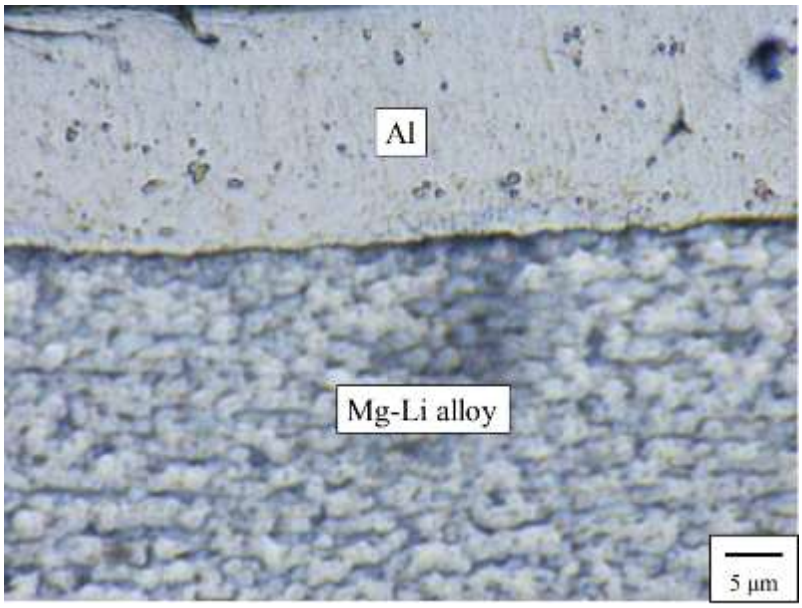

Fig. 6.8 No IMC can be observed at the Al/Mg-Li alloy interphase after deformed to fracture at 0.001 s^{-1} at 423 K.

6.3.3 Mechanism of the superplastic deformation

6.3.3.1 Strain rate sensitivity index

The superplastic deformation can be described by the following equation [6.1]:

$$\dot{\varepsilon} = \frac{ADG\boldsymbol{b}}{kT}\left(\frac{\boldsymbol{b}}{d}\right)^{p}\left(\frac{\sigma}{G}\right)^{n} \quad (6\text{-}1)$$

where $\dot{\varepsilon}$ is the strain rate, σ is the flow stress, D is the appropriate diffusion coefficient, G is the shear modulus, $\boldsymbol{b}$ is the Burgers vector, k is Boltzmann's constant, d is the grain size, T is the absolute temperature, p is the exponent of the grain size, n is the stress exponent and A is a dimensionless constant. The strain rate sensitivity index m ($m = \partial ln\sigma/(\partial ln\dot{\varepsilon}) = 1/n$) is

important in describing the behavior of superplastic deformation. Plastic flow by slip is associated with a low *m* value (*m*=0.2 or lower) while superplastic deformation by GBS is characterized by a high *m* value of about 0.5 [6.2-6.4]. Fig. 6.9 is plotted to calculate the *m* values of the ERER specimens. It is suggested that the superplastic deformation of the ERER specimen at 473 K is based on GBS, with an *m* value of 0.53. At 423 K, the *m* value decreases slightly to 0.46, where the large elongation should still be attributed to GBS.

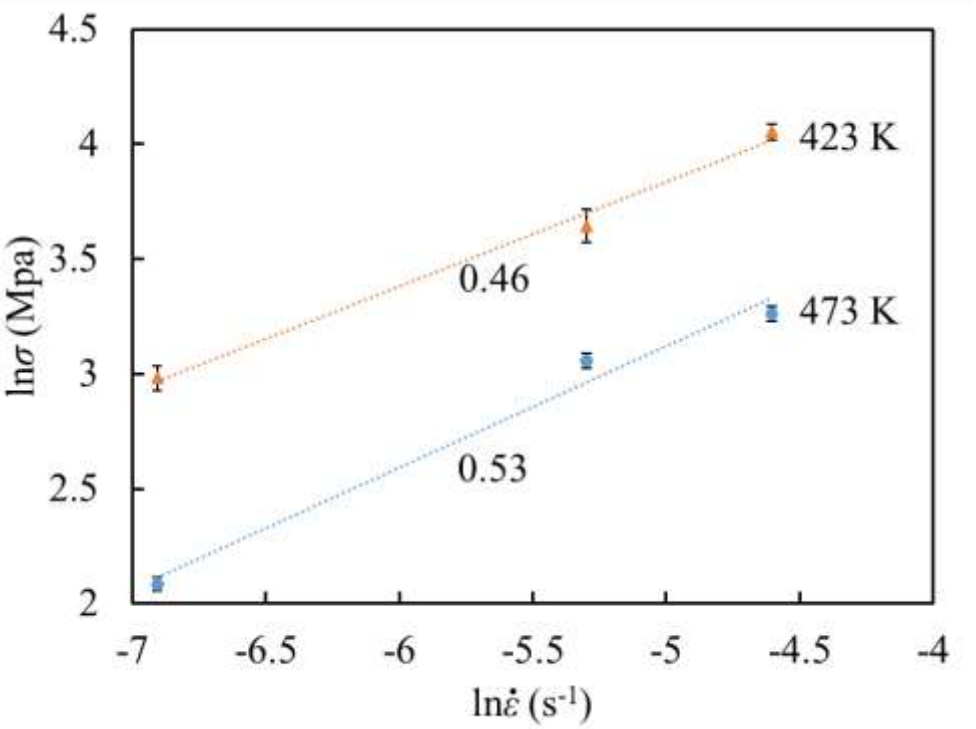

Fig. 6.9 Effects of strain rate on the flow stress of different specimens at different temperatures.

6.3.3.2 Grain structure evolution

It is generally accepted that an initial fine grain size of less than 10 μm is the requirement of GBS [6.5]. Furthermore, thermally stable fine

microstructure during the superplastic deformation is also necessary for achieving a large superplastic elongation. Namely, the grain should not grow substantially during the hot deformation. Fig. 6.10 displays the IPF maps of the ERER specimens after different levels of tensile elongation of (a) 0%, (b) 50% and (c) 100% at 473 K at 0.001 s^{-1}. Fig. 6.11 gives the corresponding grain size distributions of the specimens. The average diameters of the specimens elongated to 0, 50 and 100% are 2.8, 3.4 and 3.8 μm, respectively. Under the tensile test conditions at 473 K, the grains grow during the deformation, but the growth rate is quite slow. After an elongation of 100%, the diameters of grains are still much smaller than 10 μm which is the widely accepted maximum limit of the grain size for GBS [6.5]. Such slow grain growth is usually related to a high-density distribution of fine particles. To confirm the distribution of fine particles, the microstructure of the 100% elongated specimen was observed. As shown in Fig. 6.12 (a) and (b), many precipitates distributed at the grain boundaries. Their composition was identified to contain Mg, Li and Zn by the AES wide-scan spectrum, as shown in Fig. 6.12. This agrees with that the stable precipitate phase in the Mg-Li-Zn system is MgLiZn phase with a cubic lattice structure [6.6]. These precipitates worked as pinning particles during the superplastic deformation to prevent the grain from growing. Attributing to the fine grain size during the deformation, GBS continuously occurred and the specimens exhibited large fracture elongations.

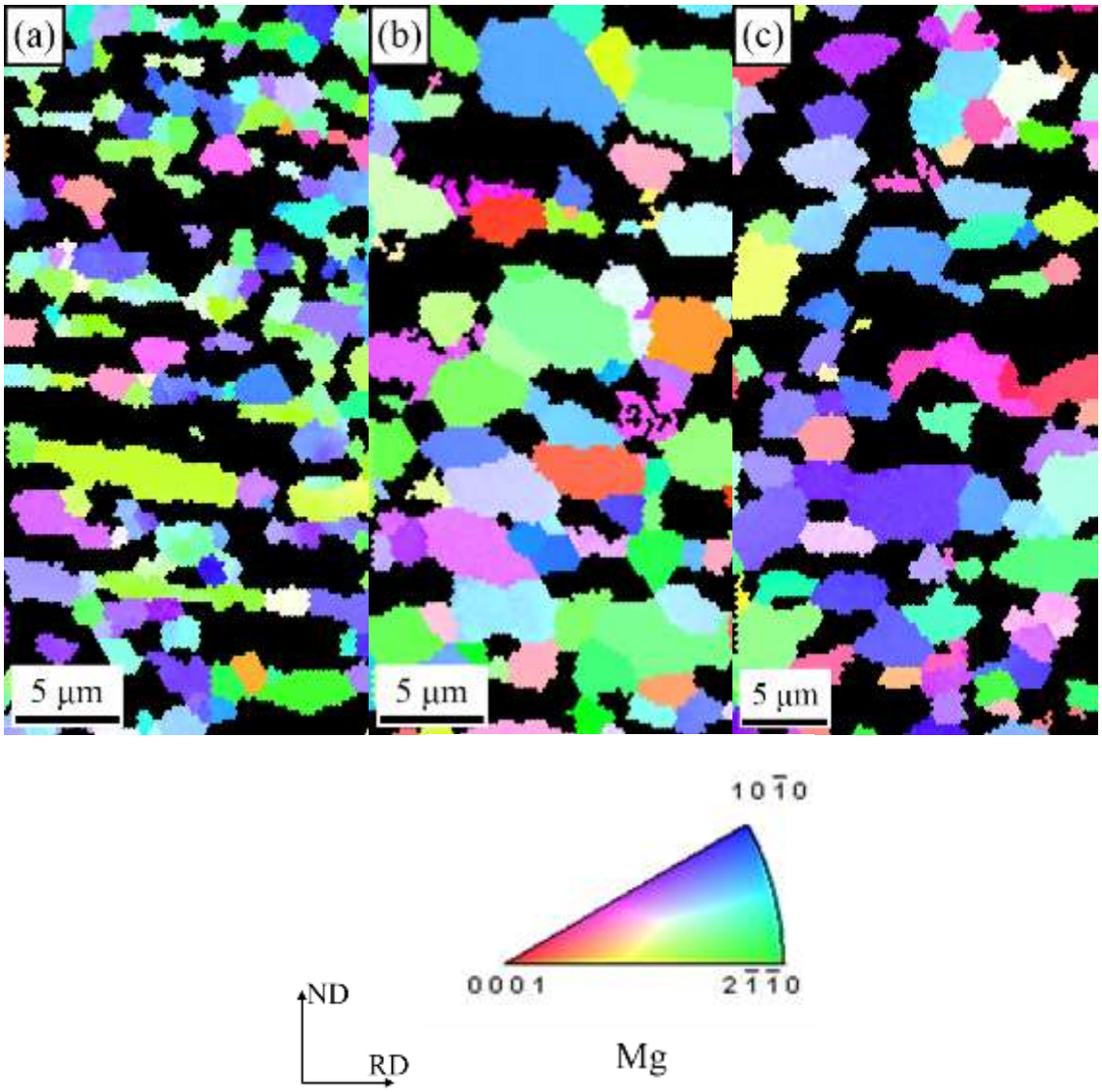
(a)
(b)
(c)
5 μm
5 μm
5 μm
$10\bar{1}0$
0001
$2\bar{1}\bar{1}0$
ND
RD
Mg

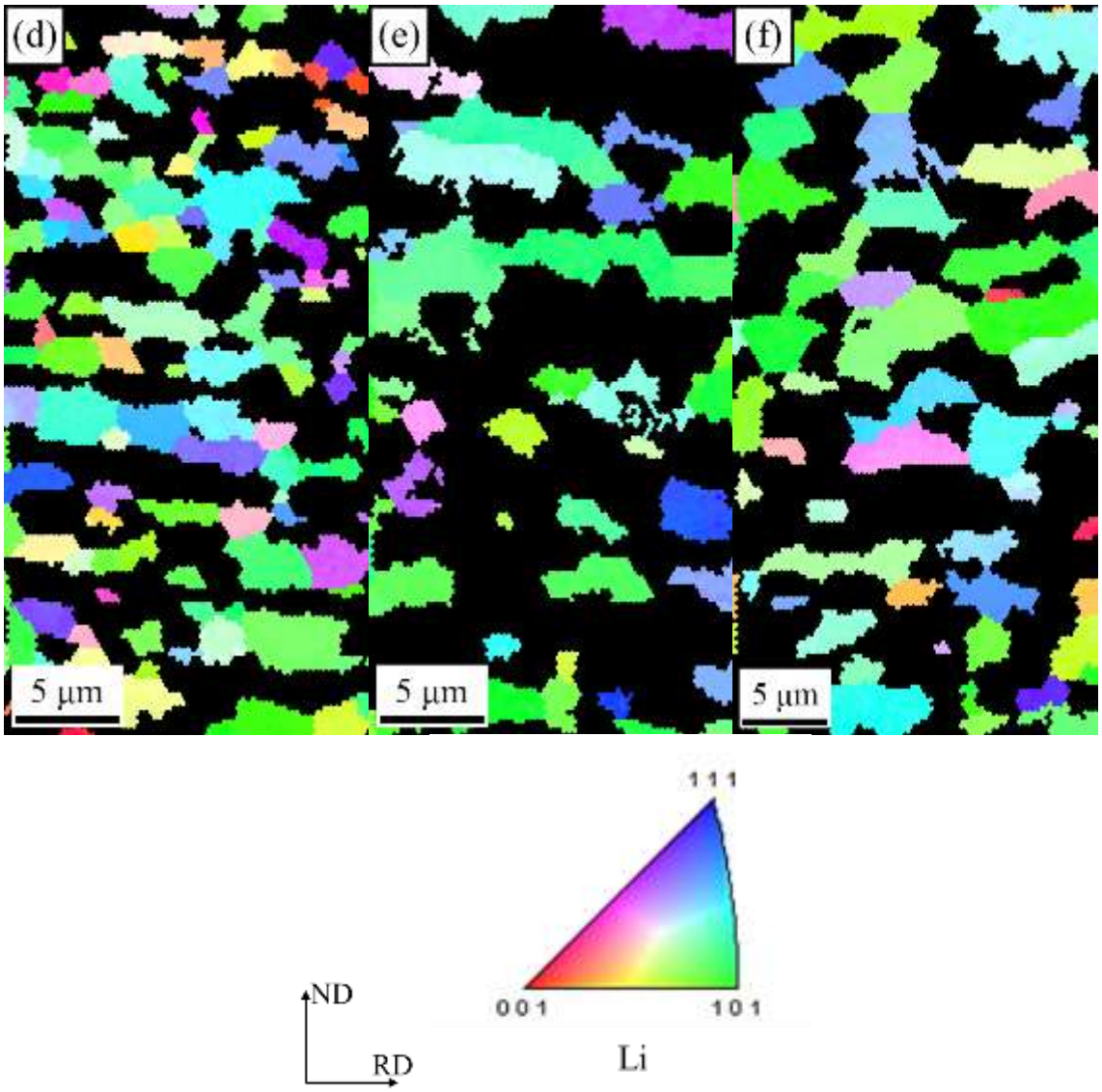

Fig. 6.10 IPF maps of the α phase in the ERER specimens after different levels of tensile elongation of (a) 0%, (b) 50% and (c) 100% at 473 K at 0.001 s^{-1}, and IPF maps of the β phase in the ERER specimens after different levels of tensile elongation of (d) 0%, (e) 50% and (f) 100% at 473 K at 0.001 s^{-1}.

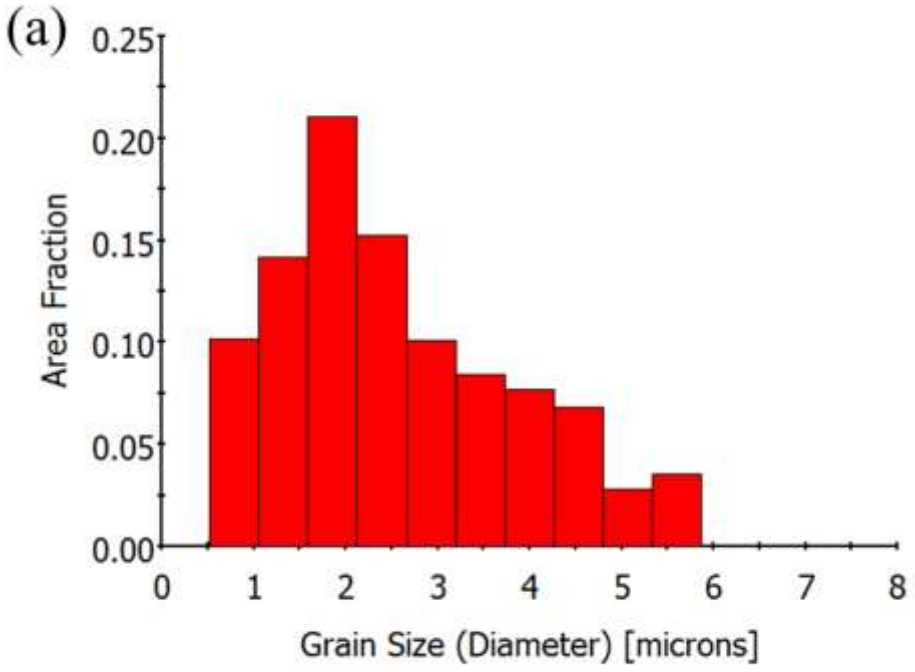
(a)
0.25
0.20
0.15
0.10
0.05
0.00
Area Fraction
0
1
2
3
4
5
6
7
8
Grain Size (Diameter) [microns]

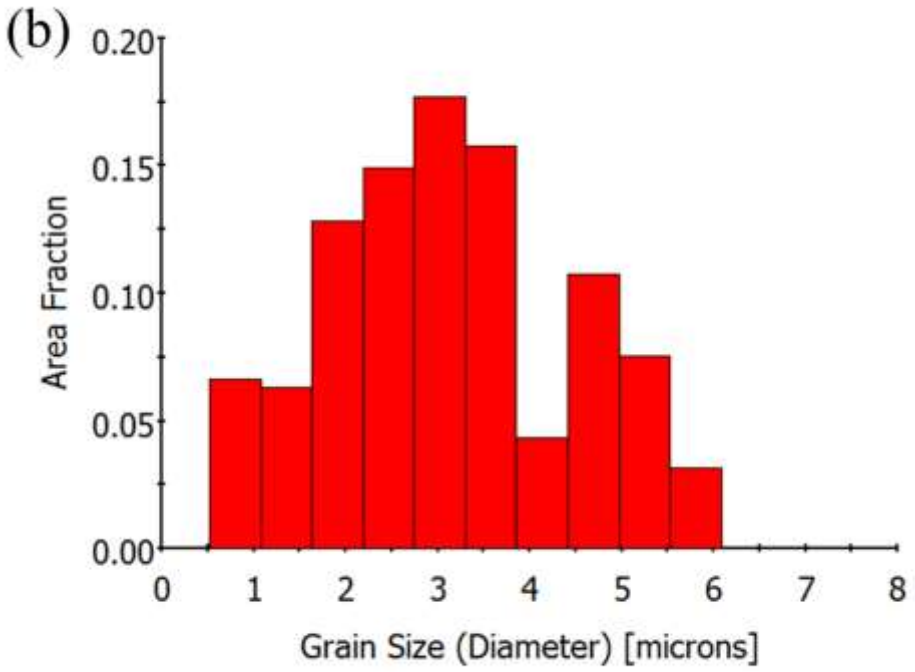
(b)
0.20
0.15
0.10
0.05
0.00
Area Fraction
0
1
2
3
4
5
6
7
8
Grain Size (Diameter) [microns]

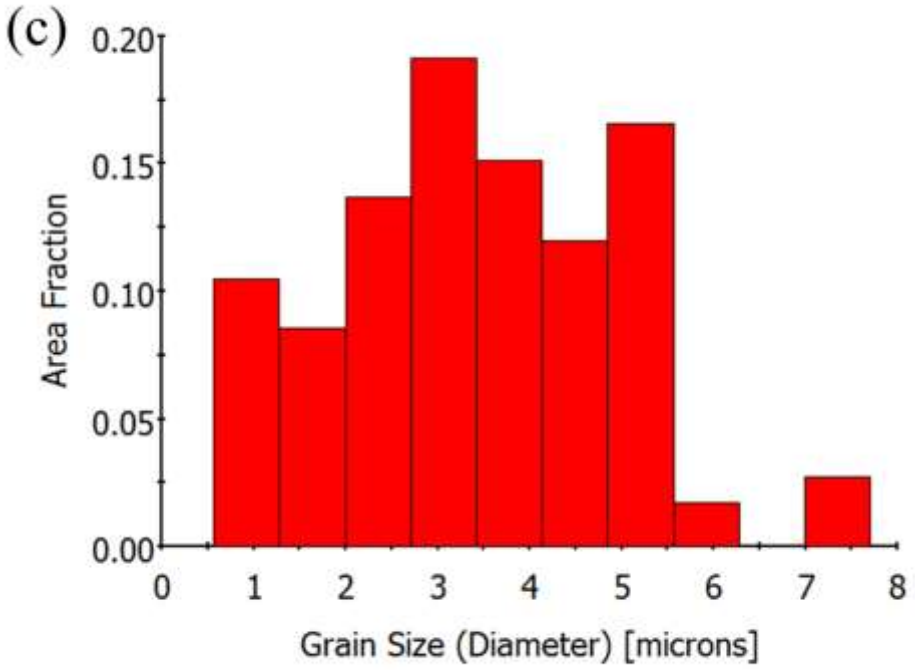

Fig. 6.11 Grain size distribution of the ERER specimens after different levels of tensile elongation of (a) 0%, (b) 50% and (c) 100% at 473 K at 0.001 s^{-1}.

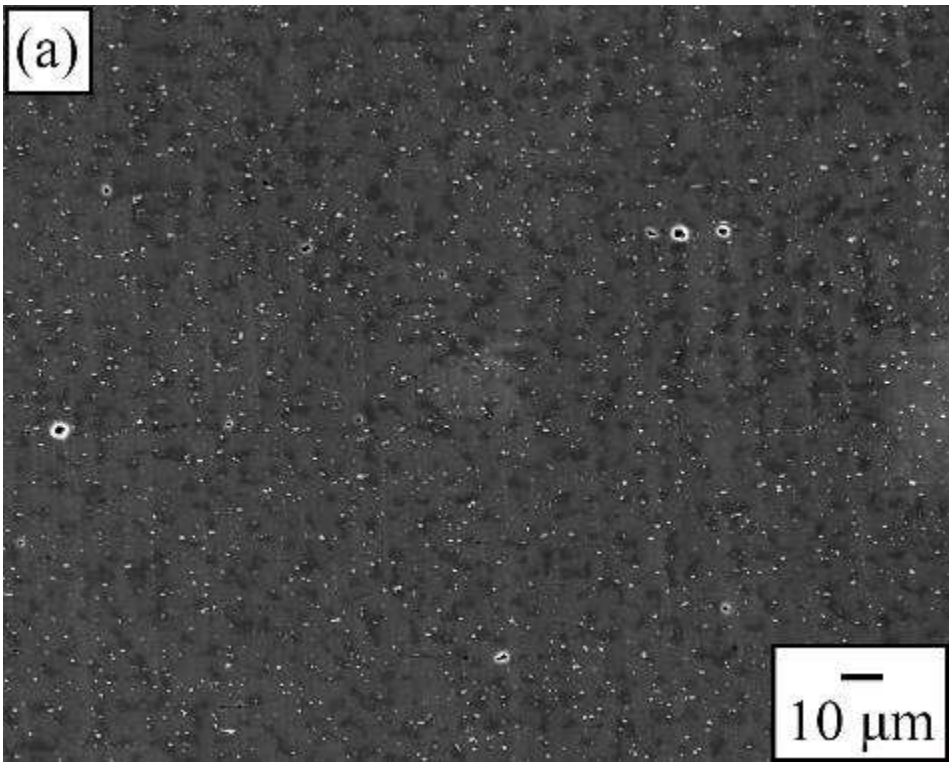
(a)
10 µm

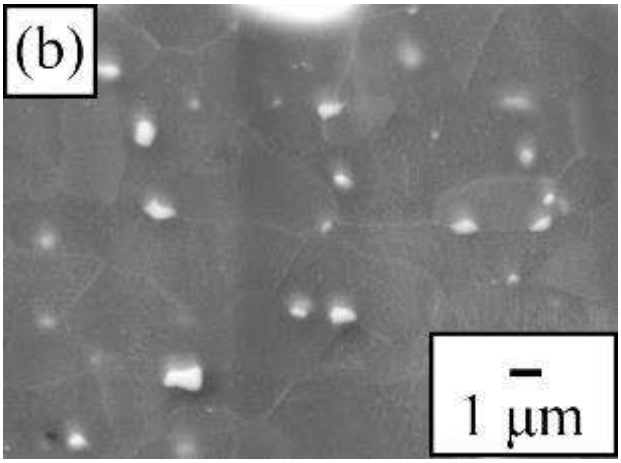
(b)
1 µm

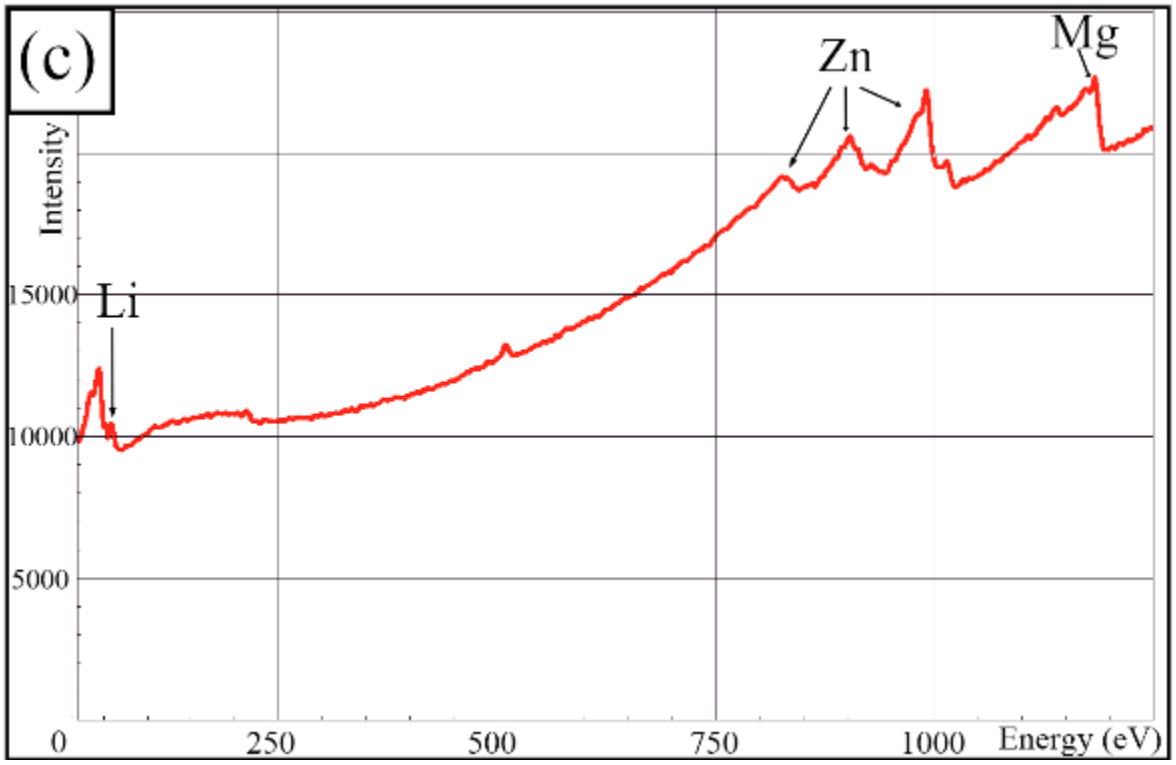

Fig. 6.12 (a) and (b) SEM pictures of the ERER specimens elongated to 100% at 473 K at 0.001 s^{-1}; (c) the wide-scan AES of the precipitate.

6.3.3.3 Texture evolution

The *m* value suggests the superplastic deformation is based on GBS at 473K. However, GBS cannot occur continuously on all boundaries without at least one accommodation process to relax stress concentrations [6.7]. Diffusion creep or intragranular dislocation glide can act as the accommodation mechanism. The sign of intragranular dislocation glide during the superplastic deformation is of interest, because the absence of it is often considered as the evidence of diffusion creep. The presence of intragranular dislocation glide can be determined by the texture analysis during the superplastic deformation, because the formation of texture is brought about

only by dislocation glide [6.8]. On the other hand, GBS usually causes a random grain rotation during the superplastic deformation [6.9], which can progressively weaken the texture during superplastic deformation [6.10-6.13]. Fig. 6.13 displays the pole figures of the (0 0 0 1) plane of α phase and the (0 0 1) plane of β phase after superplastic deformation of 0, 50 and 100%. For the HCP α phase, it shows an initial basal texture at ND due to the rolling process. After deformed to 50% as shown in Fig. 6.13 (b), the texture of the α phase becomes weaker. This should be the result of the random grain rotation. However, further texture weakening is not observed when the deformation increases to 100%, as illustrated in Fig. 6.13 (c). It is suggested that during the deformation from 50% to 100%, the grains of α phase tend to rotate to the preferential orientation, rather than random orientations. This reveals the presence of the intragranular dislocation glide in α phase during the superplastic deformation. As GBS contributes to the overall smearing of the pole density, the change of the pole intensity suggests GBS is more dominant at the early deformation stage from 0% to 50% elongation than at the stage from 50% to 100% elongation. On the other hand, it is interesting to note that the texture intensity of the β phase exhibits a very different trend compared with that of the α phase. The evolution of the (0 0 1) pole figures of the β phase are shown in Figs. 6.13 (d), (e) and (f). At the early stage from 0% to 50% elongation, the texture intensity of the β phase increases, especially at the part between RD and TD. At from 50% to 100% elongation, an overall decrease of the texture intensity is observed. Contrary to the α phase, GBS is more dominant at the later stage from 50% to 100% elongation in the β phases. The change of the maximum intensity of all the pole figures are show

in Fig. 6.13 (g), where the opposite trends of the texture changes can be observed. Therefore, in the dual-phase Mg-Li-Zn alloy, GBS is not a homogenious process and exhibits different trends of changes in the two phases.

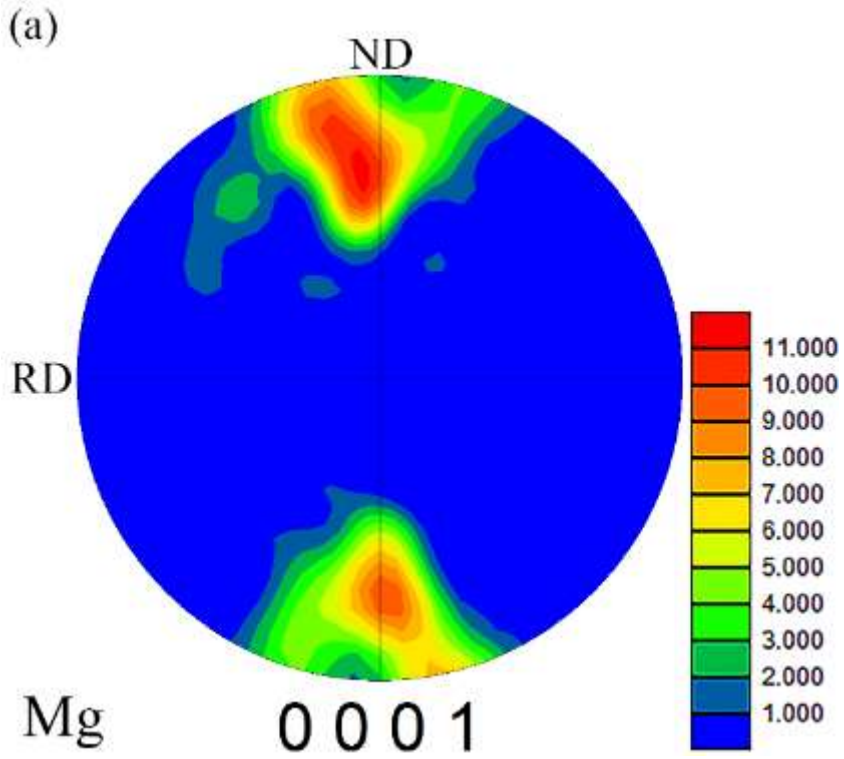

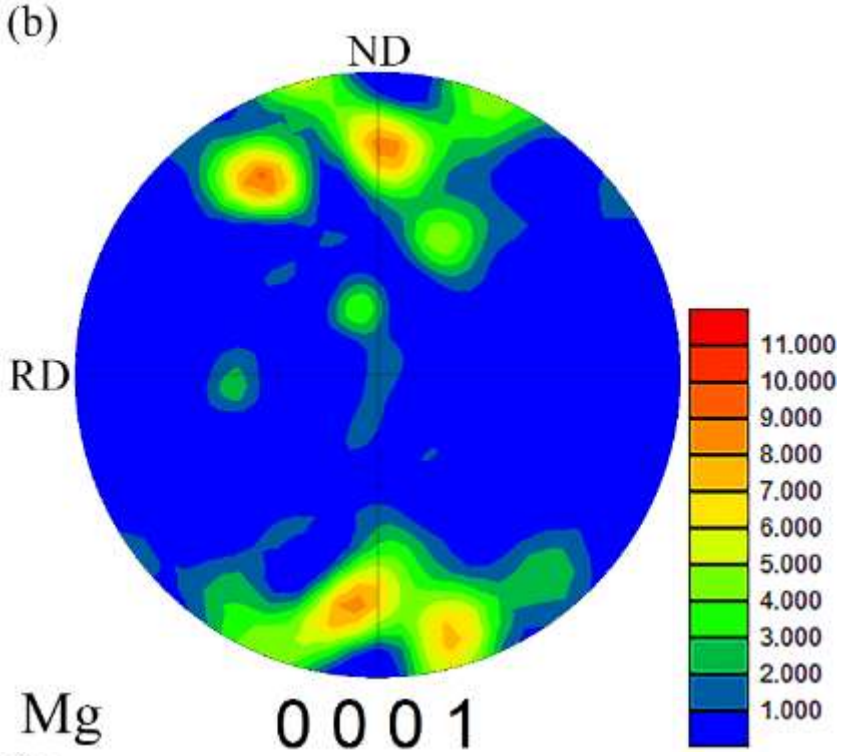
(b)
ND
RD
11.000
10.000
9.000
8.000
7.000
6.000
5.000
4.000
3.000
2.000
1.000
Mg
0 0 0 1

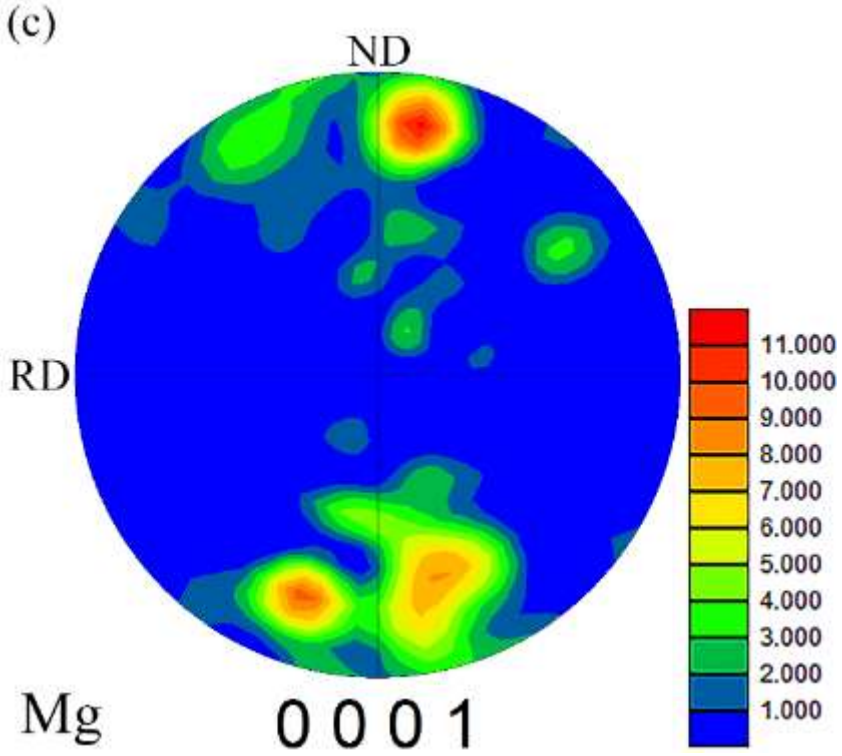
(c)
ND
RD
11.000
10.000
9.000
8.000
7.000
6.000
5.000
4.000
3.000
2.000
1.000
Mg
0 0 0 1

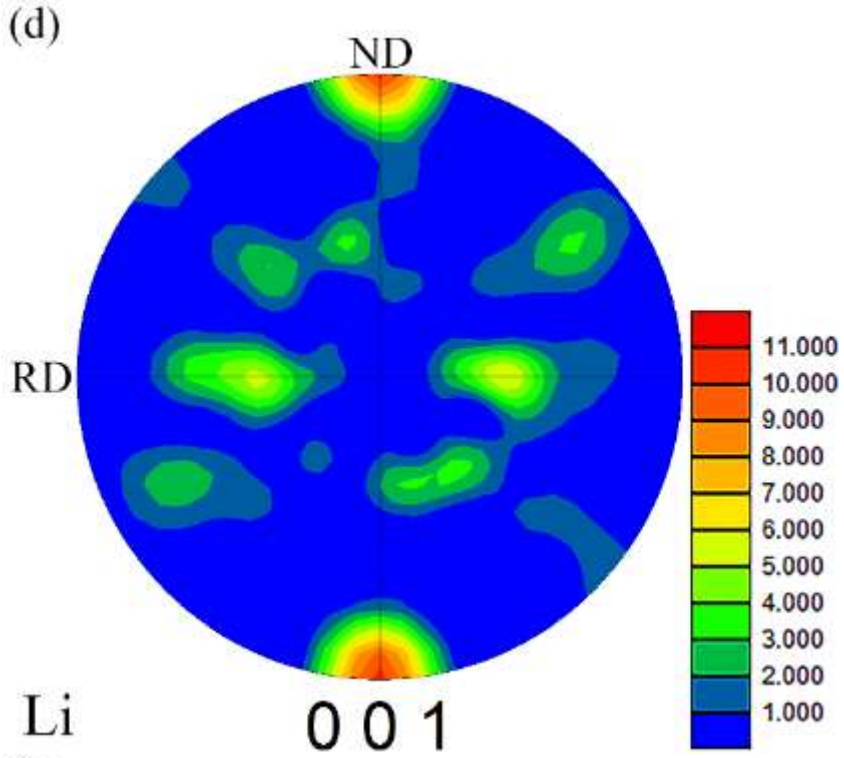
(d)
ND
RD
Li
0 0 1
11.000
10.000
9.000
8.000
7.000
6.000
5.000
4.000
3.000
2.000
1.000

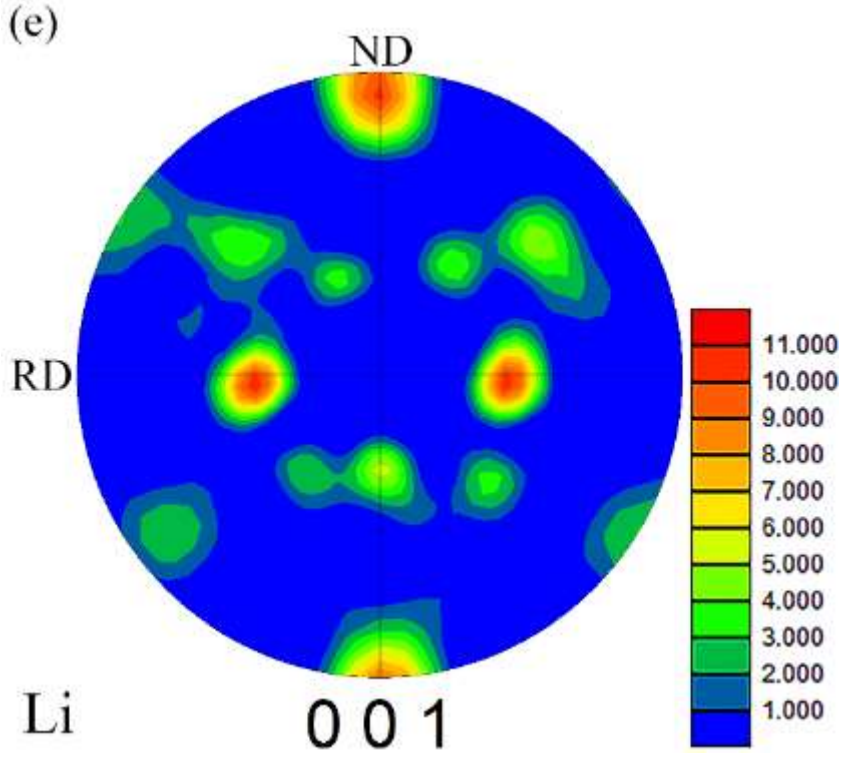
(e)
ND
RD
Li
0 0 1
11.000
10.000
9.000
8.000
7.000
6.000
5.000
4.000
3.000
2.000
1.000

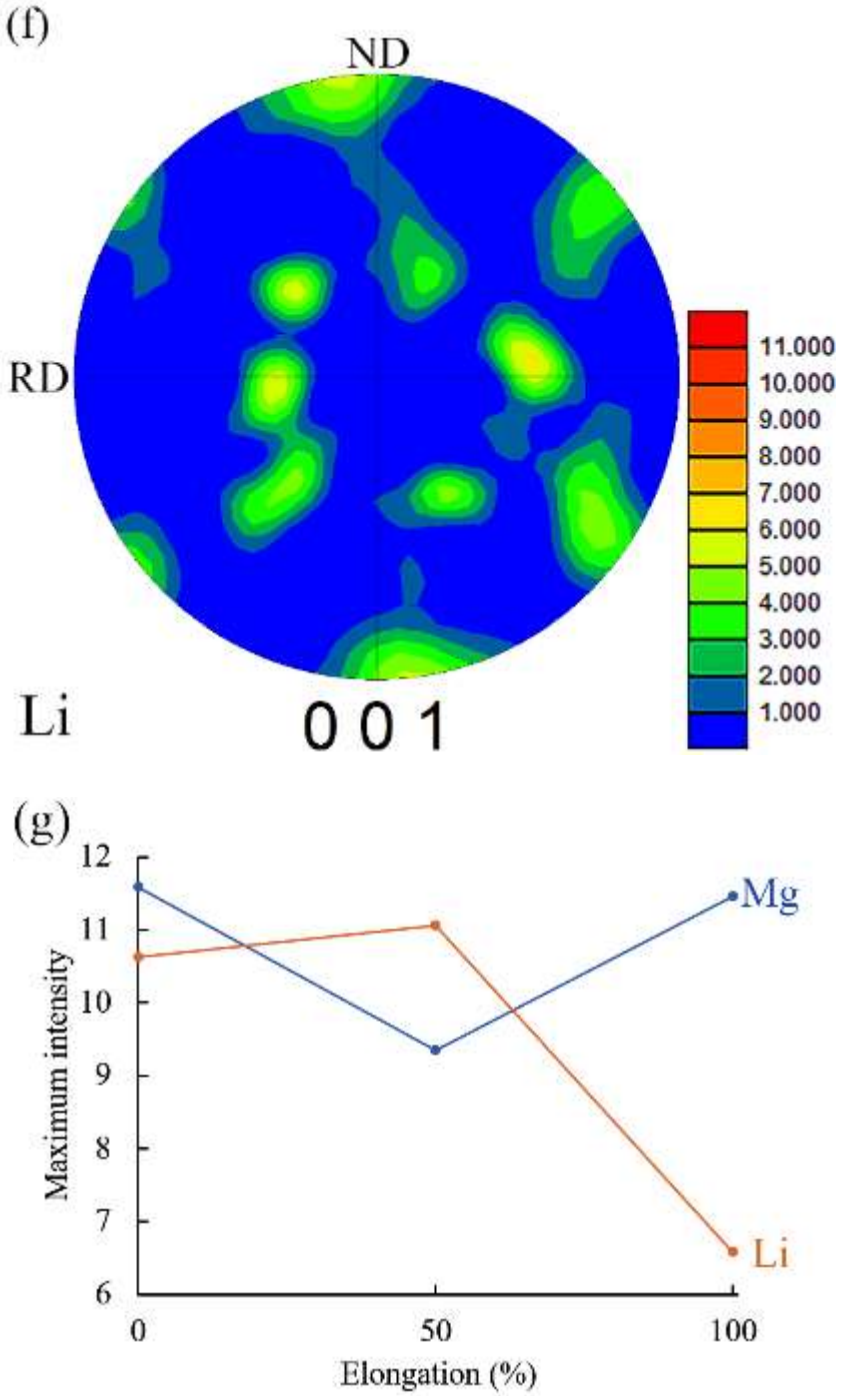

Fig. 6.13 The (0 0 0 1) pole figures of α phase in the ERER specimens after tensile elongations of (a) 0%, (b) 50% and (c) 100% at 473 K at 0.001 s^{-1}; the (0 0 1) pole figures of β phase in the ERER specimens after tensile elongations of (d) 0%, (e) 50% and (f) 100% at 473 K at 0.001 s^{-1}; and (g) the change of the maximum intensity of the pole figures.

6.4 Summary

In this chapter, by using the multi extrusion-rolling deformation process, the structure of the Mg-Li alloy was refined. Therefore, conclusions can be obtained as below.

1. A very fine and homogenous structure of the Mg-8Li-5Zn alloy was successfully processed by a multi extrusion-rolling deformation process method.

2. The Mg-8Li-5Zn alloy exhibited good superplasticity at of 473 K and 423 K. The largest elongation 1400% was observed at 0.001 s^{-1} at 473 K. Even at a quite high strain rate of 0.01 s^{-1}, 620% fracture elongation was still achieved. At low temperature of 423 K, the largest elongation was 720% at 0.001 s^{-1}. After coated with Al, the specimen can be elongated to about 400% without cracks on the coating.

3. The strain rate sensitivity of the alloys deformed at 473 K and 423 K were 0.46 and 0.53, respectively. The deformation mechanism of the Mg-8Li-5Zn alloy at 0.001 s^{-1} at 473 K was grain boundary sliding accommodated by dislocation glide. Grain boundary sliding occurred inhomogeneously in the α and β phases at different stages of the superplastic deformation.

References

[6.1] T. G. Langdon, The mechanical properties of superplastic materials, Metall. Trans. A 13 (1982) 689-701.

[6.2] P. Metenier, G. González-Doncel, O. A. Ruano, J. Wolfenstine, O. D. Sherby, Superplastic behavior of a fine-grained two-phase Mg-9wt.%Li alloy, Mater. Sci. Eng. A 125 (1990) 195-202.

[6.3] H. Somekawa, A. Kinoshita, K. Washio, A. Kato, Enhancement of room temperature stretch formability via grain boundary sliding in magnesium alloy, Mater. Sci. Eng. A 676 (2016) 427-433.

[6.4] H. Matsunoshita, K. Edalati, M. Furui, Z. Horita, Ultrafine-grained magnesium-lithium alloy processed by high-pressure torsion: Low-temperature superplasticity and potential for hydroforming, Mater. Sci. Eng. A 640 (2015) 443-448.

[6.5] M. Kawasaki, T. G. Langdon, Review: achieving superplasticity in metals processed by high-pressure torsion, J. Mater. Sci. 49 (2014) 6487-6496.

[6.6] A. Yamamoto, T. Ashida, Y. Kouta, K. B. Kim, S. Fukumoto, H. Tsubakino, Precipitation in Mg-(4-13) %Li-(4-5) %Zn ternary alloys, Mater. Trans. 44 (2003) 619-624.

[6.7] K. Matsuki, Y. Uetani, M. Yamada, Y. Murakami, Superplasticity in an Al-6 wt.-%Mg alloy, Met. Sci. 10 (1976) 235-242.

[6.8] O. A. Kaibyshev, B. V. Rodionov, R. Z. Valiev, Peculiarities of dislocation slip during superplastic deformation of Zn-Al alloys, Acta Metal. 26 (1978) 1877-1886.

[6.9] M. T. Pérez-Prado, G. González-Doncel, O. A. Ruano, T. R. Mcnelley, Texture analysis of the transition from slip to grain boundary sliding in a discontinuously recrystallized superplastic aluminum alloy, Acta Mater. 49 (2001) 2259-2268.

[6.10] K. A. Padmanabhan, J. Hirsch, K. Lücke, Superplasticity-dislocation creep interactions in a coarse grained Al-Cu-Zr alloy, J. Mater. Sci. 26 (1991) 5309-5317.

[6.11] J. W. Edington, K. N. Melton, C. P. Cutler, Superplasticity, Prog. Mater. Sci. 21 (1976) 61-170.

[6.12] K. A. Padmanabhan, Grain boundary sliding controlled flow and its relevance to superplasticity in metals, alloys, ceramics and intermetallics and strain-rate dependent flow in nanostructured materials, J. Mater. Sci. 44 (2009) 2226-2238.

[6.13] J. A. del Valle, O. A. Ruano, Separate contributions of texture and grain size on the creep mechanisms in a fine-grained magnesium alloy, Acta. Mater. 55(2007) 455-466.

Chapter 7 Conclusions

Mg alloys are potential structural metal materials which can meet the compelling need for weight-reduction and energy-efficiency in industry, because of the lowest density of Mg among all structural metallic materials. Also, Mg alloys possess other attractive properties such as high specific stiffness and good castability. In spite of these advantages, the critical problems that restrict a wide industrial application of Mg alloys are their poor corrosion resistance and bad formality. The conventional coating methods do not work well on Mg alloys because of the high chemical reactivity of Mg. In this study, the author aims to give a corrosion-resistant Al coating on Mg alloy by a hot extrusion method, which is proved to be an effective and efficient coating method for Mg alloy.

To produce a better formability of Mg alloy, a special class of Mg alloy, dual-phase Mg-Li alloy was focused on in this study, because adding Li in Mg can change the lattice structure for HCP to BCC. Moreover, the possible superplasticity after structure refinement of this alloy system was also noted, which was believed to be an effective way to form Mg alloys. Three Mg-Li alloys with different Zn concentrations were used: Mg-8wt% Li (LZ80), Mg-8wt% Li-2wt% Zn (LZ82) and Mg-8wt% Li-5wt% Zn (LZ85).

In chapter 1, the background of the study was introduced and the necessity of improving the corrosion resistance and formability of Mg alloys was illustrated.

From chapters 2 to 4, taking LZ80 alloy as a sample, the fabrication and characterization of the Al-coated Mg-Li sheet were demonstrated.

In chapter 2, the hot extrusion coating technique was explained. By this method, an Al-coated LZ80 alloy rectangular bar was successfully fabricated. A well bonded Al coating was produced with a uniform thickness of approximately 200 μm. The Al-coated LZ80 alloy bar exhibited excellent corrosion resistance in a 0.5 mass% HCl aqueous solution, which is the same as the corrosion resistance of pure Al.

In chapter 3, the extruded Al-coated LZ80 alloy bar was deformed into sheet by hot rolling. After rolled into thin sheet, the coating kept a uniform thickness and the bonding between the coating and substrate remained free from cracks. The Al-coated LZ80 alloy sheet still exhibited excellent corrosion resistance in a 0.5 mass% HCl aqueous solution.

In chapter 4, the tensile properties of the Al-coated LZ80 alloy sheet was investigated. The as-rolled Al-coated LZ80 alloy sheet exhibited a fracture elongation of about 35% at room temperature at 0.001 s^{-1} with no break at the bonding between the substrate and coating. At 573 K the as-rolled Al-coated LZ80 alloy sheet exhibited elongation of about 200% at 0.001 s^{-1} in the air. Refining of the structure was thought to be the key point to get a better superplasticity.

In chapter 5, the tensile properties of the Al-coated LZ82 and LZ85 alloy sheets were demonstrated. The addition of Zn brought about obvious improvements of room temperature tensile properties, especially large improvement of strength was observed with the use of LZ85 alloy. Therefore,

for the best comprehensive mechanical properties, LZ85 was selected for the subsequent study.

In chapter 6, by using the multi extrusion-rolling deformation process proposed in this study, the structure of the Mg-Li alloy was significantly refined. A remarkably fine and homogenous dual-phase structure was successfully processed. After the multi extrusion-rolling deformation process, the alloy exhibited excellent superplasticity. The largest elongation of 1400% was observed at 0.001 s^{-1} at 473 K. Even at a higher strain rate and a lower temperature, large elongations were still observed. When coated with Al, the specimen was elongated to about 400% without cracks on the coating. The strain rate sensitivity of the alloys deformed at 423 K and 473 K were 0.46 and 0.53, respectively. The deformation mechanism at 0.001 s^{-1} at 473 K was grain boundary sliding accommodated by dislocation glide. Grain boundary sliding occurred inhomogeneously in the α and β phases at different stages of the superplastic deformation.

Finally, by the multi extrusion-rolling deformation process, a corrosion-resistant and deformable Mg alloy can be produced, which is expected to solve the critical problems of Mg alloy. The technique originally developed in this study would contribute more or less to the development of the application of Mg alloys.

Acknowledgements

I would like to express my appreciation to all those who give help in the completion of this thesis.

Firstly, I would like to appreciate mg supervisor, Professor Kiyotaka Matsuura in Hokkaido University. He gave me a lot of guidance, knowledge and support during the whole period of my doctoral program. Without his help, this thesis would not have been completed.

I would like to thank Professor Munekazu Ohno in Hokkaido University. He gave me a lot of precious comments which often inspired me.

I would also give my thanks to Professor Toko Tokunaga. Her kind advices and guidance helped me a lot in my research work.

I would like to thank Professor Seiji Miura and Professor Ken-ichi Ikeda in Hokkaido University for their comments and advices during my study.

I would like to express thanks to Professor Zhang Milin, Professor Wu Ruizhi and Mr. Zheng Haipeng in Harbin Engineering University for the help in casting Mg-Li alloys.

I would like to thank Mr. Keita Suzuki in the Laboratory of XPS analysis in Hokkaido University for his technical supports.

I would like to give thanks to all my labmates and friends. They gave me much help in study and daily life.

I would like to appreciate my family for their understanding and support.

Finally and gratefully, I would like to express my appreciation to CSC for the financial support to help me complete my doctoral program.